

Contents lists available at ScienceDirect

Petroleum Science

journal homepage: www.keaipublishing.com/en/journals/petroleum-science



Original Paper

Evaluation of dynamic inter-well connectivity by using the statevariable-capacitance model



Li-Wen Guo ^a, Shi-Yuan Qu ^b, Yuan-Yuan Lei ^a, Zhi-Hong Kang ^a, Shuo-Liang Wang ^{a,*}

- ^a School of Energy Resources, China University of Geosciences, Beijing, 100083, China
- ^b CNPC Engineering Technology R&D Company Limited, Beijing, 100083, China

ARTICLE INFO

Article history: Received 27 June 2024 Received in revised form 13 May 2025 Accepted 14 May 2025 Available online 14 May 2025

Edited by Yan-Hua Sun

Keywords:
Capacitance model
Inter-well connectivity
Time-lag coefficient
Connected volume
Reservoir simulation

ABSTRACT

During oilfield development, a comprehensive model for assessing inter-well connectivity and connected volume within reservoirs is crucial. Traditional capacitance (TC) models, widely used in interwell data analysis, face challenges when dealing with rapidly changing reservoir conditions over time. Additionally, TC models struggle with complex, random noise primarily caused by measurement errors in production and injection rates. To address these challenges, this study introduces a dynamic capacitance (SV-DC) model based on state variables. By integrating the extended Kalman filter (EKF) algorithm, the SV-DC model provides more flexible predictions of inter-well connectivity and time-lag efficiency compared to the TC model. The robustness of the SV-DC model is verified by comparing relative errors between preset and calculated values through Monte Carlo simulations. Sensitivity analysis was performed to compare the model performance with the benchmark, using the Qinhuangdao Oilfield as a case study. The results show that the SV-DC model accurately predicts water breakthrough times. Increases in the liquid production index and water cut in two typical wells indicate the development time of ineffective circulation channels, further confirming the accuracy and reliability of the model. The SV-DC model offers significant advantages in addressing complex, dynamic oilfield production scenarios and serves as a valuable tool for the efficient and precise planning and management of future oilfield developments.

© 2025 The Authors. Publishing services by Elsevier B.V. on behalf of KeAi Communications Co. Ltd. This is an open access article under the CC BY-NC-ND license (http://creativecommons.org/licenses/by-nc-nd/4.0/).

1. Introduction

In the development of oilfields, water injection has been shown to effectively increase oil recovery rates (Tetteh et al., 2020; Mwakipunda et al., 2023). Water injection is preferred due to its easy access to resources, relatively low cost, and ease of implementation (Ogbeiwi et al., 2018; Rini et al., 2021). The impact of water injection on enhancing oil recovery depends on the interaction between the aquifer and oil reservoir and the volume of water injected. Efficient management of water-injected oil fields relies on quickly identifying the distribution of injected fluids and accurately assessing inter-well connectivity to improve the sweeping efficiency in the secondary recovery (Hani Binti et al., 2020; Zhou et al., 2022). An accurate evaluation of the connection between wells is crucial for comprehending the fluid's

* Corresponding author.

E-mail address: wangshuoliang@cugb.edu.cn (S.-L. Wang).

dynamic behavior in the reservoir to optimize field recovery and economic efficiency (Artun, 2017; Thiam and Nakhaee, 2023). The characterization of inter-well connections is categorized into two main groups: static data analysis techniques and dynamic data analysis methods (Zhang et al., 2023).

The static data analysis methods mainly utilize static data, such as geological, seismic, and static fluid parameters, combined with geological and mathematical models to estimate injection-production relationships. They mainly include the stratigraphic comparison of electric logging data and the comparison of reservoir parameters of each well (Wohl et al., 2019; Llanes et al., 2022). In contrast, dynamic data analysis methods rely heavily on the collected real-time or historical dynamic data, such as bottomhole flow pressure and flow rate, to assess inter-well connectivity through dynamic modelling or simulations. Dynamic data analysis methods mainly include inter-well tracer technology, geochemical methods, numerical simulation, and other dynamic analysis methods derived from the inversion of inter-well connectivity based on injection and production data (Sheng et al., 2021; Huang

S. et al., 2023; Huang Z. et al., 2023).

Dynamic data analysis methods are superior to static data analysis methods in many ways. Unlike static methods, dynamic data methods can more accurately reflect the actual production conditions and dynamic changes in the reservoir. Dynamic methods utilize real-time production and monitoring data to analyze the reservoir's dynamic response and full lifecycle evolution (Liu et al., 2020; Gong et al., 2021). Among the many dynamic data analysis methods, well-testing and tracer techniques achieved quantitative interpretation based on the idealized and complex theoretical-mathematical models, which may differ significantly from the subsurface reality. In addition, these methods need to be based on static reservoir understandings, such as small layer comparisons and reservoir parameter interpretation, which usually involve longer study times and higher costs. Among geochemical techniques, the method of mineralization analysis is associated with a high level of uncertainty due to numerous influencing factors. Numerical simulation methods are mainly handicapped by the authenticity of data, particularly geological information, and the consideration of reservoir heterogeneity (Cheng et al., 2020; Shan et al., 2022).

Among the methods for identifying dynamic inter-well connectivity, the capacitance modelling method stands out. This approach was derived from the inversion of inter-well relationships based on injection and production data, and it excels in calculating inter-well connectivity. Moreover, based on the principle of material balance, the capacitance modelling method effectively takes into account the time lag characteristics and reveals the essential characteristics of the injection and production system. The time-lag coefficient, a key indicator during the derivation of the capacitance model, reflects the attenuation of the injection and production signals, assuming that a pair of injection and production wells is equivalent to a pair of input and output signals (Zhao et al., 2016). Capacitance models apply to primary, secondary, and tertiary oil recovery processes and can be used to calculate oil-water ratios and optimize injected fluid distribution at the end of oilfield development (Holanda et al., 2018; Nugroho et al., 2023).

Capacitance models can be subdivided into different categories, of which the most influential is the capacitance-resistance model, which has been extensively used in oilfield development and enhanced oil and gas recovery technologies since it was proposed by Yousef et al. (2006). Initially, the main use of the capacitanceresistance model was to quantify the connectivity between injection and recovery wells in oil fields and the effectiveness of water injection (Yousef et al., 2006). Thereafter, the model was improved to make it more adaptable to oilfield environments where injection wells are frequently shut down (Sayarpour et al., 2007). In 2009, Sayarpour et al. (2009) developed a variety of forms such as capacitance-resistance model tank (CRMT) and capacitance-resistance model producer (CRMP) to meet different accuracy requirements. In 2011, Nguyen et al. (2011) further extended the application of the capacitance-resistance model by proposing a new methodology for the estimation of inter-well connectivity in the primary and secondary recovery phases). Subsequently, in 2012, Izgec and Kabir (2012) developed an injection-recovery connectivity model for new oil fields.

In terms of enhanced oil and gas recovery technologies, capacitance models are widely used in a variety of approaches, including CO₂ drive (Sayarpour, 2008; Eshraghi et al., 2016), alternating water injection gas drive (Laochamroonvorapongse et al., 2014), and synchronized water injection gas drive (Nguyen, 2012). In addition, capacitance models have shown their potential for application in CO₂ sequestration and geothermal reservoir modelling (Tao and Bryant, 2012, 2013, 2015; Akin, 2014),

as well as in the field of low-salinity water drive (Zivar et al., 2022). More recently, Parra et al. (2024) proposed the capacitance resistance aquifer-fractional flow model (CRMPAF) in 2024, a new approach for conventional unsaturated reservoirs in primary production. Overall, capacitance model and its derivative models have significant significance in the conventional oil and gas industry and new areas like geothermal energy and CO₂ storage.

Despite the progress made in the above studies, some challenges and shortcomings still remain for the popularity of traditional capacitance models, as summarized below.

- (1) Constrained by static parameters: although the capacitance model uses historical data to assess the dynamic relationships between wells, the inter-well connectivity coefficient (λ) and time-lag coefficient (τ) in the model are usually treated as constants. Such treatment may not accurately reflect the true dynamics of oilfield evolution over time. Therefore, such models may have limitations in dynamically monitoring and predicting oilfield performance.
- (2) Lack of functionality: traditional capacitance models are insufficient in dealing with the dynamic non-homogeneity of the field due to long-term development and the ineffective water circulation (IWC) problem in the high waterbearing stage, especially in predicting the trend of water breakthrough, identifying the IWC channels and evaluating the dynamic development of different well groups. Dynamic connectivity volumes for injection and production well pairs are extremely challenging.
- (3) Limitations in data processing: capacitance models have limitations in processing complex data containing noises and adapting to changes in altered environments. In particular, when analyzing dynamically changing data, traditional capacitance models are often unable to capture changes at each time step effectively. These models typically provide a static value based on historical production data, whereas the proposed new model (which will be presented later) can calculate a value for each time step (daily, monthly, or annually), allowing for a more accurate representation of real-time changes. Therefore, there exists a need for advanced data processing techniques that can analyze dynamic changes swiftly and improve model adaptability in uncertainties.

To address the above limitations, this study proposes a new state-variable-based dynamic capacitance (SV-DC) model, which effectively overcomes these shortcomings by incorporating the extended Kalman filter (EKF) and other advanced techniques. The specific innovations are as follows.

- (1) Dynamic identification of inter-well connectivity: traditional capacitance models treat inter-well connectivity coefficients and time-lag coefficients as constants, which fail to accurately reflect the dynamic nature of oilfield evolution over time, thus limiting their ability to dynamically monitor and predict oilfield performance. The proposed SV-DC model introduces the EKF processing mechanism, enabling dynamic identification of inter-well connectivity coefficients and time-lag coefficients, allowing these parameters to change with the actual evolution of the oilfield. This innovation overcomes the limitations of static parameters in traditional capacitance models and improves the model adaptability to dynamic changes in the oilfield, enhancing the accuracy of predictions.
- (2) Dynamic identification and evaluation of ineffective water circulation channels (IWCs): traditional capacitance models

are insufficient in addressing the non-homogeneity of fields resulting from long-term development and the issue of IWCs in the high water-cut stage, particularly in predicting water breakthrough trends, identifying IWCs, and evaluating the dynamic development of different well groups. The SV-DC model, by incorporating the dynamic calculation of inter-well connectivity volumes, enables real-time identification and evaluation of IWCs. This innovation allows for the dynamic tracking of changes in connectivity volumes between well groups and provides a scientific basis for optimizing water injection strategies and improving recovery rates.

(3) Dynamic data processing and real-time updating capabilities: the SV-DC model incorporates the EKF and uses a Taylor expansion to linearize the nonlinear measurement equations, thus enabling efficient real-time dynamic estimation. Under noisy conditions, the model demonstrates good adaptability and stability, effectively responding to data fluctuations and environmental changes. Compared with traditional methods, the EKF significantly enhances the model's real-time performance, accuracy, and adaptability in dynamic data environments.

In this study, a new SV-DC is established to fill the above knowledge and technology gaps. The SV-DC model is an extension of the traditional capacitance (TC) model, by introducing the EKF processing, which not only enables the model to predict the interwell connectivity but also optimizes the estimation results based on the observed data and model predictions. The superiority of the SV-DC model is demonstrated by comparisons between the pure state-variable (SV) model and the TC model. The robustness and stability of the SV-DC model were validated through Monte Carlo simulations under different scenarios. To validate the modelling accuracy, the SV-DC model was finally applied to the Qinhuangdao Oilfield 32-6 for a practical case study, analyzing the tracer test results and the liquid productivity index in a series of well groups at the early, middle, and late stages. Overall, the SV-DC model presented in this paper can be used as a powerful tool to evaluate the connectivity between well groups and identify IWCs.

2. Construction of the SV-DC model

2.1. The TC model

The TC model effectively captures the dynamic relationships between injectors and producers, making it a valuable tool for reservoir management. Considering a reservoir with N_i injectors and N_j producers, the total mass balance equation is as follows (Sayarpour et al., 2009):

$$C_t V_{ij} \frac{d\overline{P}_{ij}}{dt} = \lambda_{ij} Q_{wi}(t) - Q_{ij}(t) \tag{1}$$

where C_t represents the compressibility, bar^{-1} ; V_{ij} denotes the pore volume, m^3 ; Q_{ij} and \overline{P}_{ij} are the flow rate (m^3/d) and the average pressure (bar) between injector i and producer j; Q_{wi} is the injection rate of injector i, m^3/d ; λ_{ij} is a proportionality coefficient that reflects the degree of influence of injector i on producer j, known as the inter-well connectivity coefficient.

$$Q_{ij} = J_j \left(\overline{P_{ij}} - P_{wfj} \right) \tag{2}$$

where J_j is the productivity index of the production well, m³/d/bar; P_{wfj} is the bottom-hole flowing pressure of the production well,

bar; $\overline{P_{ij}}$ is the average pressure between injection well i and production well j, bar. By taking the time derivative of Eq. (2), we obtain

$$\frac{dQ_{ij}}{dt} = J_j \left(\frac{d\overline{P_{ij}}}{dt} - \frac{dP_{wfj}}{dt} \right)$$
 (3)

$$\frac{d\overline{P_{ij}}}{dt} = \frac{dQ_{ij}}{I_i dt} + \frac{dP_{wfj}}{dt}$$
(4)

Substituting Eq. (4) into Eq. (1), it yields

$$C_t V_{ij} \left(\frac{\mathrm{d}Q_{ij}}{J_i \mathrm{d}t} + \frac{\mathrm{d}P_{\mathrm{wf}j}}{\mathrm{d}t} \right) = \lambda_{ij} Q_{\mathrm{w}i}(t) - Q_{ij}(t) \tag{5}$$

Eq. (6) links the pore volume (connectivity volume) V_{ij} and τ_{ij} (Yousef et al., 2006):

$$\tau_{ij} = \frac{C_t V_{ij}}{J_i} \tag{6}$$

where τ_{ij} is the first order system's time constant. This value is crucial because it indicates how quickly the reservoir responds to changes in injection rates. Although calculated as a static parameter, τ_{ij} varies dynamically in real reservoir conditions. Combining Eqs. (5) and (6) yields

$$\tau_{ij}\frac{\mathrm{d}Q_{ij}}{\mathrm{d}t} = \lambda_{ij}Q_{wi}(t) - Q_{ij}(t) - \tau_{ij}J_{j}\frac{\mathrm{d}P_{wfj}}{\mathrm{d}t} \tag{7}$$

After reviewing the method used by previous researchers (Kang et al., 2014a), it has been observed that as producer bottom pressure fluctuates much less than the production rate, the influence of the pressure term can be regarded as a secondary factor. Consequently, Eq. (7) can be simplified into

$$\tau_{ij} \frac{\mathrm{d}Q_{ij}}{\mathrm{d}t} = \lambda_{ij} Q_{wi}(t) - Q_{ij}(t) \tag{8}$$

Solving the differential equation for Eq. (8) yields

$$Q_{ij}(t) = Q_{ij}(t_0)e^{-\frac{t-t_0}{\tau_{ij}}} + \int_{t_0}^{t} \frac{\lambda_{ij}}{\tau_{ii}} Q_{wi}(\zeta)e^{-\frac{t-\zeta}{\tau_{ij}}} d\zeta$$

$$\tag{9}$$

Taking into account that the total production rate $Q_j(t)$ is the combined contributions from all injectors N_i to the producer j, the total production rate $Q_i(t)$ can be expanded as

$$Q_{j}(t) = \sum_{i=1}^{N_{i}} Q_{ij}(t) = \sum_{i=1}^{N_{i}} Q_{ij}(t_{0}) e^{\frac{-(t-t_{0})}{\tau_{ij}}} + \sum_{i=1}^{N_{i}} \lambda_{ij} \frac{e^{-\frac{t}{\tau_{ij}}}}{\tau_{ij}} \int_{t_{0}}^{t} e^{\frac{\zeta}{\tau_{ij}}} Q_{wi}(\zeta) d\zeta$$
(10)

Then Eq. (10) can be discretized with monthly intervals. $Q_{ij}(t_0)$ is the production rate of production well j at initial time t_0 , m^3/d ; $Q_{wi}(\zeta)$ is the injection rate of injection well at the time ζ , m^3/d . The first term on the right of the equals sign is a time-dependent variable correlated with the initial production, and decays exponentially over time as

$$\beta_{j}(n) = \sum_{i=1}^{N_{i}} Q_{ij}(0) e^{-\frac{n}{r_{ij}}}$$
(11)

Thus, the discretized form of Eq. (10) is given by

$$Q_{j}(n) = \beta_{j}(n) + \sum_{i=1}^{N_{i}} \lambda_{ij} \sum_{m=n_{0}}^{m=n} \frac{1}{\tau_{ij}} e^{\frac{m-n}{\tau_{ij}}} Q_{wi}(m)$$
 (12)

where $Q_j(n)$ represents the total production of production well j in time step n; $\beta_j(n)$ refers to the base liquid production rate, m^3/d ; n_0 is the initial time; m and n are the time step indexes.

The above derivation process is well documented elsewhere (Kang et al., 2014b) and lays the theoretical foundation of the TC model. In the TC model, the time-lag coefficient τ_{ij} is a dimensionless time constant representing the transfer time between wells. The TC model shows that the cumulative production of a producer is determined by the combined effect of its initial cumulative production and the historical injection activity. However, in contrast to the original work, this study introduces EKF method to dynamically estimate the time-lag coefficient and the inter-well connectivity coefficient. The capacitance model serves as the foundation for dynamic updates in the following formula derivations, breaking the static assumptions of the traditional model by introducing state variables.

The basic assumptions of the SV-DC model include that the inter-well connectivity coefficient and time-lag coefficient are dynamic, changing with factors such as injection-production activities and pressure variations during oilfield development. We

variable model based on pressure impulse responses was established and solved by the EKF algorithm (Liu and Mendel, 2007). Liu's method, i.e., the SV model, will also be compared with our proposed SV-DC and TC models, forming an integrating part of the model comparison conducted in this work. Model characteristics and modelling schemes are summarized in Table 1.

In the SV-DC model, three state variables that appear in Eq. (12) β_j , λ_{ij} , and τ_{ij} are defined and extracted as state variables since they are the key parameters controlling the dynamic response characteristics of a reservoir. These variables are integral to the model and can be effectively estimated using the EKF algorithm. Consequently, Eq. (12) can be transformed by a 3×1 state vector $\mathbf{x}_i(m)$:

$$\mathbf{x}_{i}(m) = [\mathbf{x}(m), \ \mathbf{x}_{1}(m), \ \mathbf{x}_{2}(m)]' = [\beta_{j}(m), \ \lambda_{ij}(m), \ \tau_{ij}(m)]'$$
(13)

where $\beta_j(m)$ refers to the base liquid production rate at time step m, which is initially correlated with the production at m=0 and decays exponentially over time, as described in Eq. (11); $\lambda_{ij}(m)$ represents the inter-well connectivity coefficient; $\tau_{ij}(m)$ represents the time-lag coefficient for the inter-well system. Using standard techniques, the state variables are

$$\begin{cases}
\mathbf{x}_{i}(n) = \begin{bmatrix} x(m) \\ x_{i1}(m) \\ x_{i2}(m) \end{bmatrix} + n_{xi}(m) \\
p_{i}(n) = \begin{bmatrix} 1 & \sum_{m=n_{0}}^{n} \frac{1}{\tau} e^{\frac{m-n}{\tau_{ij}}} Q_{wi}(m) & \sum_{i=1}^{N_{i}} \lambda_{ij} \sum_{m=n_{0}}^{n} \left(-\frac{1}{\tau_{ij}^{2}} e^{\frac{m-n}{\tau_{ij}}} Q_{wi}(m) - \frac{m-n}{\tau_{ij}^{2}} e^{\frac{m-n}{\tau_{ij}}} Q_{wi}(m) \right) \end{bmatrix} \mathbf{x}_{i}(n)
\end{cases}$$
(14)

assume that fluid behavior in the oilfield is complex and dynamic, and therefore, real-time updates through state variables are necessary.

Next, we aggregate the state variables for all injectors, forming a complete 1 + 2N state vector, where N is the number of injectors:

$$\mathbf{x}_{i}(m) = \left[\beta_{j}(m), \ \lambda_{1j}(m), \ \tau_{2j}(m), \ \tau_{2j}(m), \ \cdots, \ \lambda_{Nj}(m), \ \tau_{Nj}(m)\right]'$$
(15)

2.2. State variables of the capacitance model

The construction of the new SV-DC model in this study begins with the extraction of state variables by the EKF algorithm; the theoretical basis can be found in previous work where a state-

This equation represents the state variables for the entire system, incorporating both injectors and producers, as given in Eq. (16):

Table 1Comparison of TC, SV, and SV-DC models.

Model type	Calculation parameters	Identification range	Method principle
	Inter-well connectivity, time-lag coefficient Inter-well connectivity	Static identification (unique result) Dynamic time step identification (days/ months/years)	Capacitance model; (TC) linear EKF; non-linear
SV-DC model	Inter-well connectivity, time-lag coefficient, inter-well connected volume	Dynamic time step identification (days/months/years)	Capacitance model and EKF; combines linear and non-linear approaches

$$\begin{cases}
\mathbf{x}(n) = \begin{cases}
x_1(m) \\
x_{11}(m) \\
x_{12}(m) \\
x_{21}(m) \\
x_{22}(m) \\
\vdots \\
x_{N1}(m) \\
x_{N2}(m)
\end{cases} + n_x(m) \\
\vdots \\
x_{N1}(m) \\
p(n) = p_1^c(n) + p_2^c(n) \cdots + p_N^c(n) + n_p(n) = \mathbf{H}x(n) + n_p(n)
\end{cases}$$
(16)

To find the measurement matrix \mathbf{H} in Eq. (16), one needs to linearize the measurement equation (denoted as h) from Eq. (12) using a Taylor series expansion. Let Eq. (12) be written as h, and by performing the linearization, it yields

$$\varepsilon = \frac{\partial h}{\partial x} \tag{17}$$

This equation represents the first derivative of the measurement equation with respect to the state variables. The linearization process is necessary to capture the relationship between the state variables and the reservoir dynamics in a form that can be used in the EKF.

accuracy of reservoir monitoring and control.

The complete SV-DC for all injector subsystems is given in Eq. (16), where p(n) is the measured production rate, $n_x(m)$ and $n_p(n)$ are additive zero-mean white noises for the state and measurement equations. The treatment of the state variables in developing the SV-DC model is expounded through the streamlined logical sequence provided in Eqs. (13)–(20). For the computation outlined in Eqs. (13)–(20), applying the EKF algorithm is essential, as it shows proficiency in managing non-linearity and providing dynamic state estimation. Integrating the EKF algorithm with the state variable model enables us to dynamically characterize the well connectivity and time-lag coefficient, offering a more accurate and temporally responsive representation of reservoir dynamics.

2.3. Procedures of the EKF algorithm

The nonlinear EKF algorithm contains four stages: system prediction, establishing measurement equations, generating optimal estimates, and updating the error covariance. The workflow presented in Fig. 1 is the core idea of evaluating inter-well connectivity using the EKF algorithm (Liu and Mendel, 2007; Zhai et al., 2009; Zhai and Mendel, 2010).

2.3.1. System prediction

$$X(k|k-1) = FX(k-1|k-1) + n_X(k-1)$$
(21)

$$\varepsilon = \left[1 \sum_{m=n_0}^{n} \frac{1}{\tau} e^{\frac{m-n}{\tau_{ij}}} Q_{wi}(m) \sum_{i=1}^{N_i} \lambda_{ij} \sum_{m=n_0}^{n} \left(-\frac{1}{\tau_{ij}^2} e^{\frac{m-n}{\tau_{ij}}} Q_{wi}(m) - \frac{m-n}{\tau_{ij}^2} e^{\frac{m-n}{\tau_{ij}}} Q_{wi}(m) \right) \right]$$
(18)

$$\varepsilon' = \left[\sum_{m=n_0}^{n} \frac{1}{\tau} e^{\frac{m-n}{\tau_{ij}}} Q_{wi}(m) \quad \sum_{i=1}^{N_i} \lambda_{ij} \sum_{m=n_0}^{n} \left(-\frac{1}{\tau_{ij}^2} e^{\frac{m-n}{\tau_{ij}}} Q_{wi}(m) - \frac{m-n}{\tau_{ij}^2} e^{\frac{m-n}{\tau_{ij}}} Q_{wi}(m) \right) \right]$$
(19)

At this stage, we apply the Taylor expansion to approximate the non-linear measurement equation. This approximation simplifies the model, making it computationally feasible for real-time dynamic estimation.

$$\mathbf{H} = \begin{bmatrix} 1 & \varepsilon_1' & \varepsilon_2' & \cdots & \varepsilon_N' \end{bmatrix} \tag{20}$$

The measurement matrix \boldsymbol{H} is now ready to be incorporated into the EKF algorithm, providing the necessary linear relationship between the state variables and the observed measurements. This allows for real-time updating of the system state, improving the

$$P(k|k-1) = \mathbf{F}P(k-1|k-1)F^{T} + 0$$
(22)

where X is a representation of the set of state variables in Eq. (15); X(k|k-1) denotes the prediction of the current step's state variables using the state variables from the last step; \mathbf{F} is the state transition matrix of the system; $n_X(k-1)$ is the system noise. Overall, Eq. (21) uses the optimal estimate X(k-1|k-1) from the last step, the system matrix \mathbf{F} , and the noise n_X to predict the state variables at the current step.

To further highlight the advantages in autoregressive at each

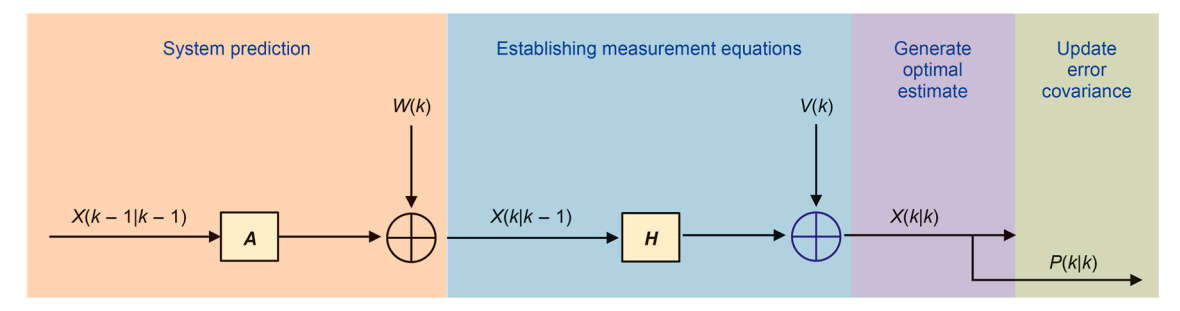


Fig. 1. Flowchart of the process of calculating inter-well connectivity using the EKF algorithm.

step provided in the EKF algorithm, m in Eq. (12) is represented by k-1 and n is represented by k.

Similarly, Eq. (22) uses the optimal estimate P(k|k-1) from the last step (P is the error covariance of the optimal estimate), the system matrix \mathbf{F} , and Q (Q is the covariance matrix of noise n_X) to predict the error covariance of the optimal estimate at the current step P(k|k-1).

The state transition matrix \mathbf{F} is a $3N \times 3N$ Jacobian matrix, the explicit form of which is given below for the non-linear state equation in Eqs. (23) and (24):

$$\boldsymbol{F}_{X} = \begin{bmatrix} \boldsymbol{A}_{1} & \underline{0} & \cdots & \underline{0} \\ \underline{0} & \boldsymbol{A}_{2} & \ddots & \vdots \\ \vdots & \ddots & \ddots & \underline{0} \\ \underline{0} & \cdots & \underline{0} & \boldsymbol{A}_{N} \end{bmatrix}$$
 (23)

$$\mathbf{A}_{i} = \begin{bmatrix} 1 & 0 & 0 \\ 0 & 1 & 0 \\ 0 & 0 & 1 \end{bmatrix} \tag{24}$$

2.3.2. Establishment of the measurement equation

The measurement equation describes the relationship between the state variables and the actual observations. For the system state variable X(k), one can observe the variable associated with Z(k), as expressed as

$$Z(k) = \mathbf{H}X(k) + n_{p}(k) \tag{25}$$

where *Z* is the observed value of the variables; \boldsymbol{H} is the observation matrix; n_p is the measurement noise.

2.3.3. Optimal estimation generation

The generation of optimal estimation mainly consists of calculating the Kalman gain (Eq. (26)) and establishing the optimal estimate equation (Eq. (27)).

$$K_{\mathbf{g}}(k) = \frac{P(k|k-1)\mathbf{H}^{\mathrm{T}}}{\mathbf{H}P(k|k-1)\mathbf{H}^{\mathrm{T}} + R}$$
(26)

$$X(k|k) = X(k|k-1) + K_{g}(k)[Z(k) - HX(k|k-1)]$$
(27)

The core idea of the EKF algorithm is to combine model predictions with actual measurements to obtain an optimal state estimate, by searching the minimum mean square of the estimation error. This process requires finding a gain K_g that minimizes the mean square of the estimation error, as expressed in Eq. (26), after a series of mathematical derivations.

Eq. (27) represents a correction based on the difference (i.e., the residual) between the predicted state variable X and the actual measurement Z. This perspective $K_{\rm g}$ determines the extent to which the predicted state variables are corrected based on the measurement residuals. It should be noted that the X(k|k-1) in the priori estimation equation differs from the X(k) in the measurement equation. X(k|k-1) is obtained from the prediction of the system state at the step k-1; whereas, X(k) is the measurement at the step k, which is independent of the values of the

measurements at the last step.

2.3.4. Error covariance update

$$P(k|k) = [1 - K_{g}(k)\mathbf{H}]P(k|k-1)$$
(28)

As the last stage of EKF algorithm, it ensures that the estimate is not only optimum but also matches the real uncertainty.

So far, three models have been introduced: the TC model, the SV model based on the EKF algorithm, and the SV-DC model by integrating the merits of the first two. The following work will compare the different performances of these three models, as shown in Table 2.

3. Comparative evaluation of model performance

The three models (TC, SV, and SV-DC models) discussed above are utilized to analyze the reservoir's complex fluid flow relationships and the interplay between injectors and producers. In reservoir analysis, these models require a complete collection of time series production data. Acquiring comprehensive production data, such as injection and production rates and bottomhole pressure (BHP), can depend on either field monitoring results or numerical simulation results. Although field-recorded data are closer to the actual operation in the reservoir, they are often subjected to disturbances from production regimes and practical operations, making it challenging to obtain complete time series information. Therefore, this study has chosen the reservoir simulator to simulate the production conditions of the oilfield.

3.1. Construction of the numerical model

In the simulation, a widely used commercial software, tNavigator, was used to simulate the performance of wells or well groups. Establishing the model and the petrophysical parameters in this paper refers to a mature oilfield in Oinhuangdao. China, which provides strong data support for the subsequent model calibration. A 3D reservoir model with 315 m \times 315 m \times 25 m (length \times width \times height) was developed, as shown in Fig. 2. The chosen permeability values (30, 100, 200, and 400 mD) for the preferential channels between the producer and injector cover a broad range of flow scenarios, enabling a detailed analysis of permeable channels on fluid mobility. The petrophysical parameters used in the model were obtained through laboratory tests and calibrated by field monitoring, and listed in Table 3. An irreducible water saturation of 32% was assumed at the beginning of reservoir development. This simulation was crucial for providing complete and reliable production data, unaffected by real-world operational disturbances such as well shut-ins, which are commonly encountered in field data. These simulation results serve as essential input for the dynamic estimation of inter-well connectivity and time-lag coefficients in the SV-DC model. Furthermore, tNavigator was used to establish models under different permeability conditions, providing insight into how permeability variations impact inter-well connectivity. The resulting production data obtained from tNavigator simulations were compared with theoretical predictions from

Table 2 Comparison of model performances.

Model type	Characteristics	Advantages
TC model SV model SV-DC model	Considers time delay effect Uses EKF for parameter estimation Combines linear relationship and state-variable estimation; connected volumes, IWCs	Convenient, clear physical meaning High-accuracy prediction and real-time update Higher robustness and accuracy, superior in complex and dynamic environments

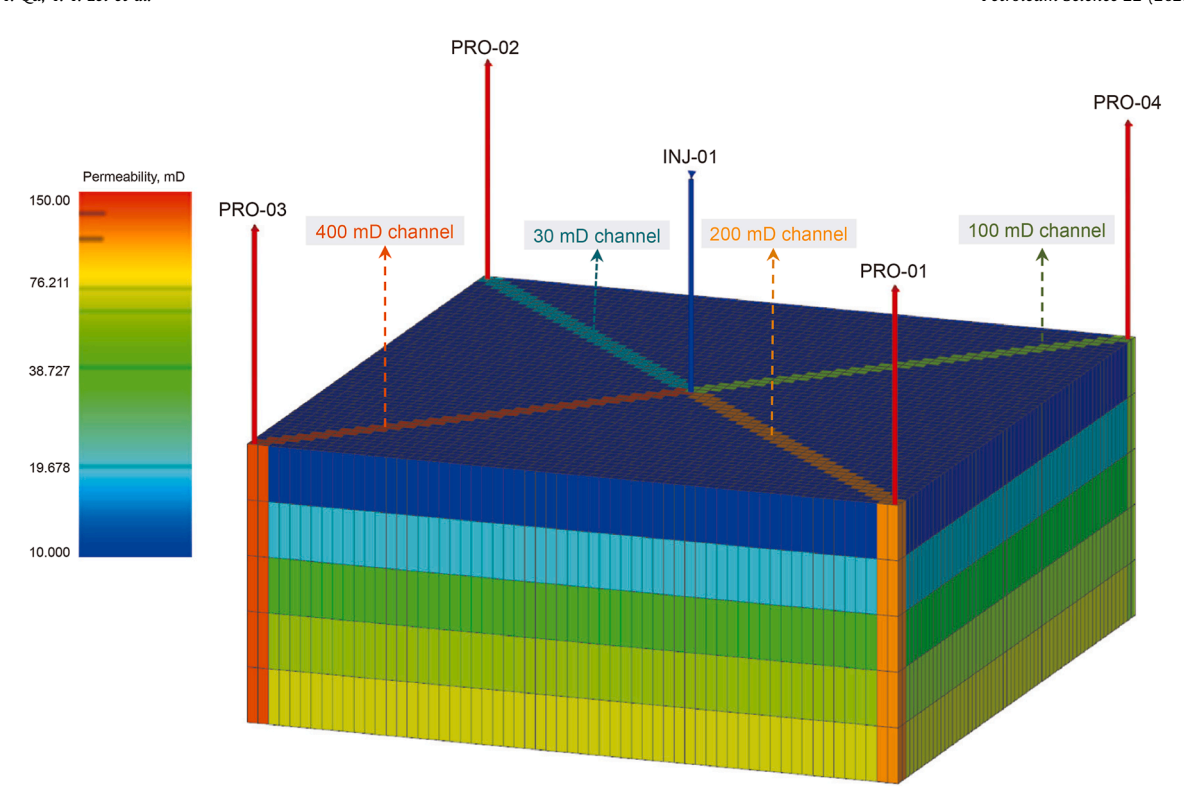


Fig. 2. The reservoir model for simulation data generation (permeability of the preferential channels between PRO-01, PRO-02, PRO-03, PRO-04, and INJ-01 are 30, 100, 200, and 400 mD, respectively, the figure has a longitudinal elongation by a factor of ten).

Table 3 Petrophysical parameters used in the model.

Parameter	Value
Porosity, %	32
Depth, m	6000
Initial water saturation, %	20
Crude oil viscosity, mPa·s	22-260
Matrix permeability, mD	20
Oil density (in situ), kg/m ³	867
Water density (in situ), kg/m ³	1000
BHP of the injector, bar	750
BHP of the producer, bar	600
Permeability of channel to PRO-01, mD	30
Permeability of channel to PRO-02, mD	100
Permeability of channel to PRO-03, mD	200
Permeability of channel to PRO-04, mD	400
Width of the high-permeability channel, m	7.1
Length of grid in the X , Y , and Z directions, m	5

the SV-DC model, ensuring the model's accuracy in representing real-world reservoir behavior.

3.2. Numerical results of water breakthrough

Fig. 3 together with Fig. 4 provide a comprehensive view of water breakthrough in four producers. Fig. 3 illustrates the declining trend in oil saturation at chronological water breakthrough times for four producers, while Fig. 4 shows the corresponding water cuts, the measurement of the relative amount of water in the producer wellhead. The numerical prediction results of water breakthroughs are highly sensitive to the selection of time steps. Shortening the time step can indeed improve accuracy, but it comes at the cost of increased time and storage requirements. By conducting a comprehensive analysis with different time steps, it

is found that the simulation results are generally stable when the time step reaches one month. The simulation period in this paper spans 121 months (2021/12–2032/01). Notably, water breakthrough events in the four producers occur on 2022/01/01, 2022/02/01, 2022/03/01, and 2022/07/01, indicating the formation of continuous water flow channels within the reservoir. This facilitates efficient water movement towards the wells along the model's diagonal, as observed in Fig. 4, where PRO-04 experiences water coming first, followed by PRO-03, PRO-02, and PRO-01.

The permeability of the preferential channels between the producers and the central injector varies, with PRO-04 possessing the highest permeability. Permeability of the preferential channel results in a greater impact on water breakthrough, as evidenced by the sequence observed in the producers at presented in Fig. 4. Historical data records the timeline of water breakthrough for each well: 210 d for PRO-01, 90 d for PRO-02, 60 d for PRO-03, and 30 d for PRO-04.

Although the breakthrough time shown in Fig. 4 is based on predictions from the numerical simulation model, it is important to note that the actual field data may be influenced by numerous uncertainties, such as well relationships and fault systems. This analysis with the results from Figs. 3 and 4 helps further validate the accuracy of the SV-DC model.

3.3. Characterization of inter-well connectivity and time-lag coefficient

Fig. 5 illustrates the inter-well connectivity computed by the three models. The results of the SV-DC model and the SV model are presented as solid and dash lines, respectively, reflecting their ability to capture the time-varying characteristics. The results of the TC model, on the other hand, are presented as three single solid dots locating at the corresponding pressure impulse moment since

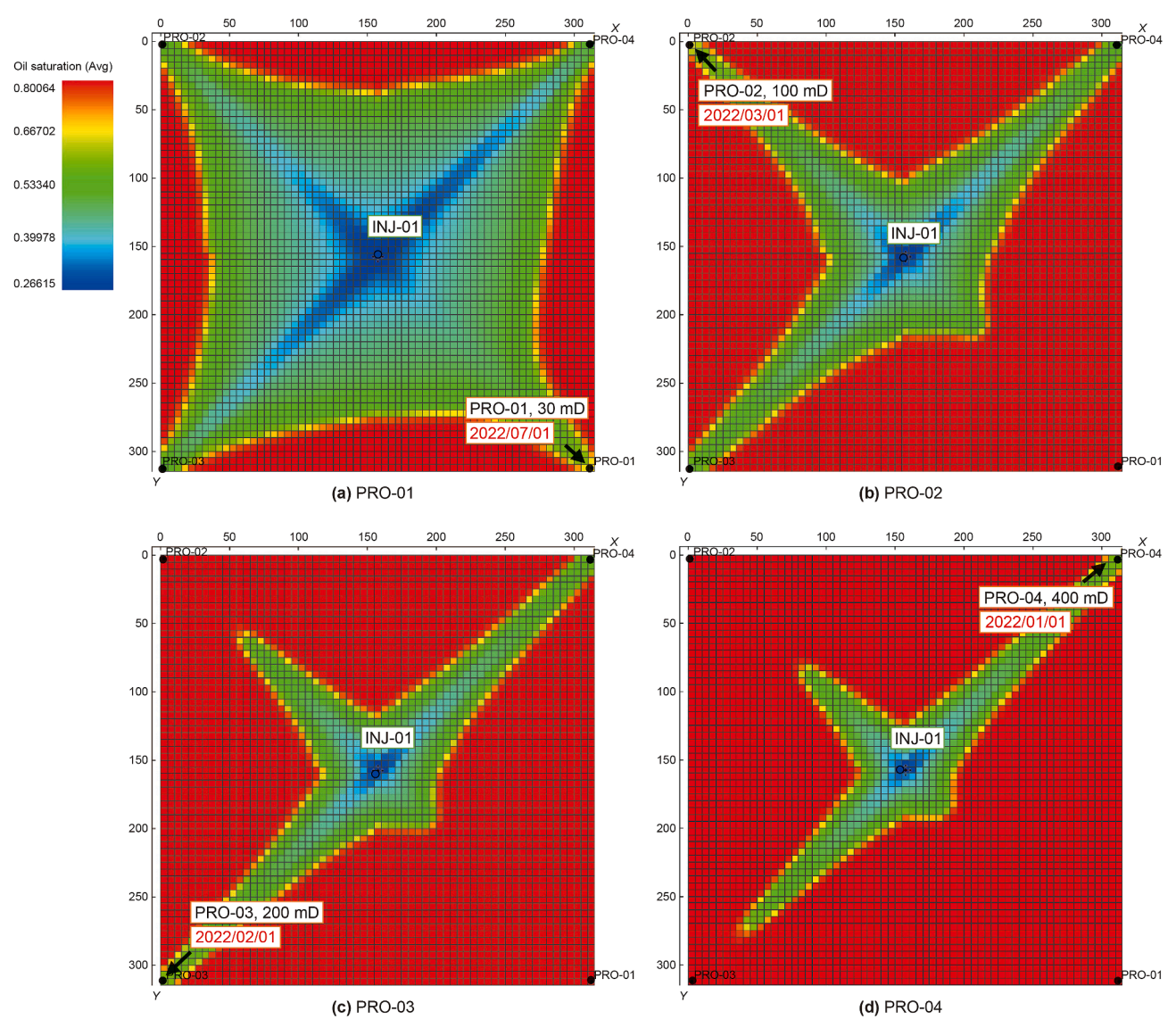


Fig. 3. The water/oil saturation distribution reflecting water breakthrough times for the four producers.

the TC model only provides a static estimate.

The calculated relative errors of the λ from the SV and SV-DC models, defined as $\frac{\lambda_{SV-DC}-\lambda_{SV}}{\lambda_{SV}}$, are 19.5% (400 mD), 18.5% (200 mD), 15.7% (100 mD), and 9% (30 mD), respectively, showing that the SV-DC model and the SV model present similar oscillation patterns in the inter-well connectivity, especially after the first pressure impulse applied at 2024/01/01. Additionally, the SV-DC model appears to be more sensitive to pressure impulses, indicating its potential advantages when facing large pressure fluctuation.

During the three pressure pulse stages (2024/01–2024/06, 2027/01–2027/06, 2031/01–2031/06), both the SV-DC and SV models show fluctuating inter-well connectivity coefficients, with similar fluctuation ranges and patterns, further validating the accuracy of the SV-DC model in simulating dynamic reservoir behavior. Notably, the SV-DC model demonstrates a more pronounced response to pressure pulses. During these stages, the inter-well connectivity coefficient follows a "rapid increase—rapid decrease—gradual stabilization—decline" pattern, reflecting the reservoir's quick response to pressure changes and subsequent adaptation. The rapid increase in connectivity occurs as the

pressure pulse is applied, followed by a decrease as the pressure wave dissipates. Once the wave stabilizes, the connectivity coefficient becomes steady, gradually decreasing to equilibrium. The peak connectivity values are proportional to the amplitude of the pressure pulse, confirming that the SV-DC model accurately captures the reservoir's dynamic response to varying pressure conditions.

Additionally, we observed significant differences in the curve trends of the SV-DC and SV models before 2022/01/01, with the SV-DC model showing a downward trend and the SV model showing an upward trend. This difference can be attributed to two main factors. On the one hand, the models have different mathematical structures: the SV model is a difference equation that focuses on recursive relationships at discrete time steps, representing a dynamic system model based on stepwise changes. In contrast, the SV-DC model is an integral effect model, representing a continuous summation relationship that aggregates the effects of multiple inputs to predict a single output. On the other hand, both models employ an EKF process. As an adaptive signal processing technique, the EKF optimization algorithm becomes increasingly accurate over time, which may cause certain data

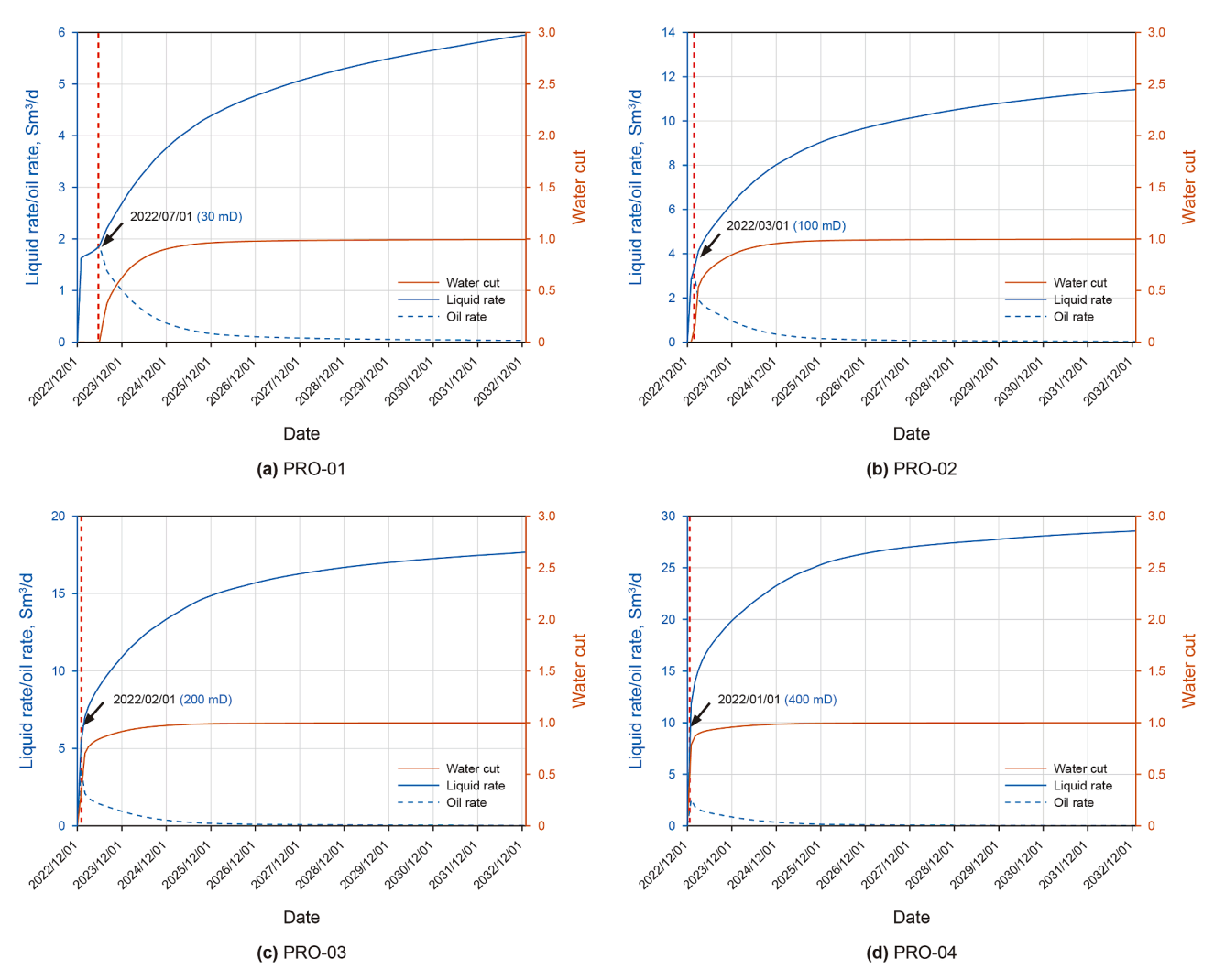


Fig. 4. Water cut variations in four producers.

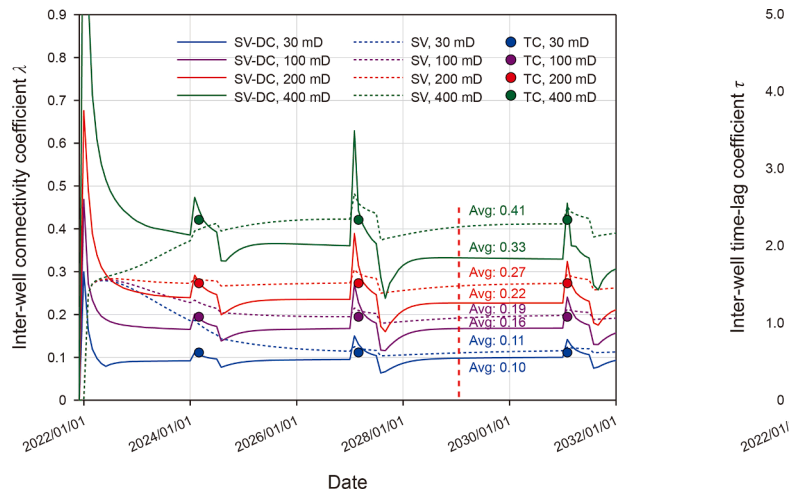


Fig. 5. Dynamic temporal variations of inter-well connectivity in SV-DC, SV, and TC models. The SV-DC and SV models provide calculated results at each time step, while the TC model produces a single result based on data from all-time steps.

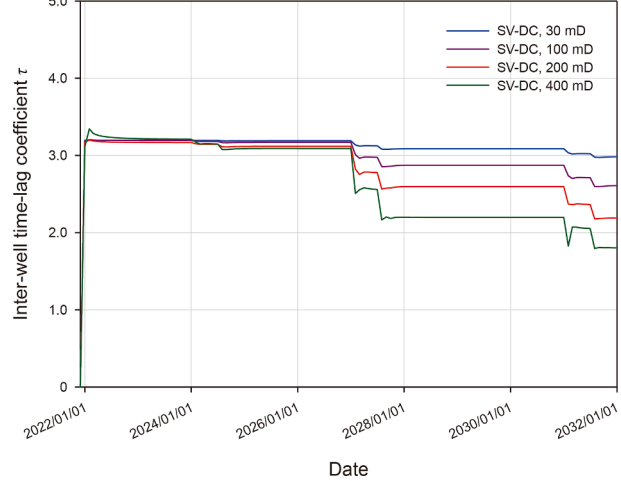


Fig. 6. Dynamic temporal variations of time-lag coefficients predicted by the SV-DC model. The figure shows that higher permeability leads to shorter time-lag coefficients, indicating faster fluid flow and earlier breakthrough at producers.

fluctuations during the early stages of the model. These fluctuations reflect the model's self-adjusting nature, and as more data accumulates, the predictions tend to become more precise. We also observed that the trends in the inter-well connectivity

coefficient curves of the SV-DC and SV models are closely related to the permeability of the high-permeability channels. This trend clearly shows that as permeability increases, the inter-well connectivity coefficient also increases, which is consistent with our understanding of reservoir characteristics. In short, high-permeability channels (e.g., 400 mD) exhibit significantly higher inter-well connectivity coefficients compared to low-permeability channels (e.g., 30 mD), thus validating the traditional understanding of reservoir fluid flow characteristics.

The time-lag coefficient characterizes the delay in fluid transfer from injectors to producers, and its definition is given in Eq. (6) (Yousef et al., 2006; Parra et al., 2023). The variation of τ over time can be attributed to changes in reservoir conditions, such as permeability, fluid viscosity, and flow pathways. These factors affect the propagation of pressure impulses. Therefore, τ can be considered a dynamic parameter that adjusts according to changes in the reservoir state. Fig. 6 describes the evolution of the time-lag coefficient τ obtained from the SV-DC model. The order in the magnitude of τ of the four producers is $\tau_{30\text{mD}} > \tau_{100\text{mD}} > \tau_{200\text{mD}} > \tau_{400\text{mD}}$. The τ values are inversely proportional to the permeability of preferential channels. This suggests that in reservoirs with higher permeability, the mobility of fluids accelerates, leading to a more rapid flow of fluids to producers. This finding is consistent with the observations made in Figs. 3 and 4 regarding the breakthrough time of the water cone. Since the fluid flow rate is directly related to the permeability, the increased mobility in the dominant channel with high permeability results in the injected water reaching the producers earlier.

Overall, the proposed SV-DC model effectively simulates the dynamic behavior of fluid flow in the reservoir, especially in terms of the acuity it exhibits in response to pressure impulses. The SV-DC model sensitively captures the variation of the inter-well connectivity λ and reveals the effect of permeability magnitude on fluid migration. The SV-DC model also quantifies the effect of fluid transfer from wells to wells through the time-lag coefficient τ .

Furthermore, in a related study (Guo et al., 2024), we carried out a series of sensitivity analyses by varying key parameters such as permeability, permeable channel width, injection pressure differentials, injection duration, and well group configuration. Although these variations led to substantial fluctuations in dynamic data (e.g., injection rate, production rate, and water cut), the results remained consistent with both field observations and numerical simulations, indicating that the model can maintain stability and reliability in complex scenarios. By examining these parameters, we demonstrated that the SV-DC model exhibits

favorable adaptability when confronted with highly variable field data

Moreover, the SV-DC model leverages the EKF to correct and update data at each time step, which minimizes the impact of initial assumptions on final computational results. This feature is crucial for sustaining robust performance, even under conditions of significant data fluctuations and uncertainties. Our sensitivity analyses further revealed that the SV-DC model can achieve stable identification accuracy despite highly fluctuating inputs, underscoring its advantages and reliability for practical applications.

4. Model robustness validation

The robustness and reliability of the proposed SV-DC model need to be verified to broaden its application, especially in simulating the dynamic behavior of fluids under complex geological and engineering conditions, to achieve the leap from the "simulator" to the "field". The SV-DC model's robustness is validated based on the synthetic data generated through Monte Carlo simulation. The reason for choosing Monte Carlo simulation is that it enables us to set the true values of λ' and τ' in advance, providing us with a known frame of reference to assess the stability of the SV-DC model in the face of interferences and noises (Liu and Mendel, 2007; Vadapalli et al., 2014).

4.1. Monte Carlo simulation

The process of testing the robustness of the SV-DC model using Monte Carlo simulation is displayed in Fig. 7. It solves for the optimal λ and τ values based on the known injection volume Q_{wi} and liquid yield Q_j . The process is as follows: the values of λ' and τ' are assumed first, and then the Q_j is calculated using the Q_{wi} with noise, as highlighted in the blue part. This part is essentially the inversion modelling process of computing Q_j by the TC model. Next, recalculate λ and τ through the SV-DC model using these calculated Q_j and Q_{wi} with noise (orange part). The purpose of this is to compare the relative errors between the recalculated λ and τ and the presets (λ' and τ'). If the calculated relative errors are less than 10% (Cremon et al., 2018), the SV-DC model is considered to have good self-robustness.

Considering conversion of the well groups often encountered in actual oilfield production, the validation under two scenarios, i.e., multiple producers and one injector, and multiple injectors and one producer, was carried out. In the former case, the production rates of three producers and the injection rate of one injector were

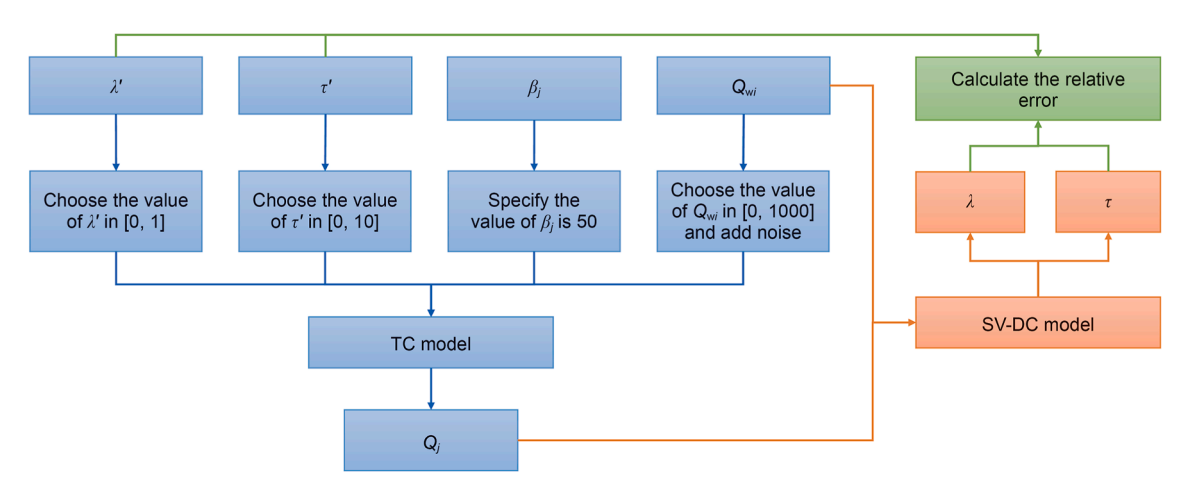


Fig. 7. SV-DC model robustness verification flowchart via Monte Carlo simulation.

selected as the synthetic data. Similarly, the synthetic data for the latter is the injection rates of three injectors and the production rate of one producer.

The specific workflow is presented in Fig. 7. Synthetic data are generated as follows.

- (1) Specify the value of Q_{wi} in [200, 800]; choose the value of λ' in [0, 1]; choose the value of τ' in [0, 10]; choose the value of β_j is 50; the number of time steps is set to 2000; the number of Monte Carlo simulations is set to 100.
- (2) Add measurement noises $n_{wi}(k)$ to $Q_{wi}(k)$ with $SNR = 10\log_{10}\left[\frac{E(Q_{wi}(k))^2}{E(n_{wi}(k))^2}\right] = 20$ dB. Generate the noise injection rates $Q_{wi}(k)$. SNR means the signal-to-noise ratio.
- (3) To generate the noise production rates Q_j , the three injectors and a single producer are implemented with noise by specifying β_j , λ' , τ' , and Q_{wi} using the procedure described above.
- (4) The noise injection rates Q_{wi} and noise production rates Q_j are obtained by down-sampling rate. Estimate using the just-generated data from the SV-DC model.
- (5) Compute the mean relative errors of λ and τ at each time k ($k = 1, 2, 3, \dots, 2000$).

$$\lambda_{\text{mean relative error}}(k) = \frac{|\lambda(k) - \lambda'(k)|}{\lambda'(k)}$$
 (29)

$$au_{\text{mean relative error}}(k) = \frac{| au(k) - au'(k)|}{ au'(k)}$$
 (30)

4.2. Simulation results for different well groups

4.2.1. Three producers and one injector

First, a well group of three producers and one injector is selected for analysis. Applying the Monte Carlo simulation, the injection and production rate data with random noise are generated, as shown in Fig. 8.

The original injection rate was set to range from 200 to 800 m³/

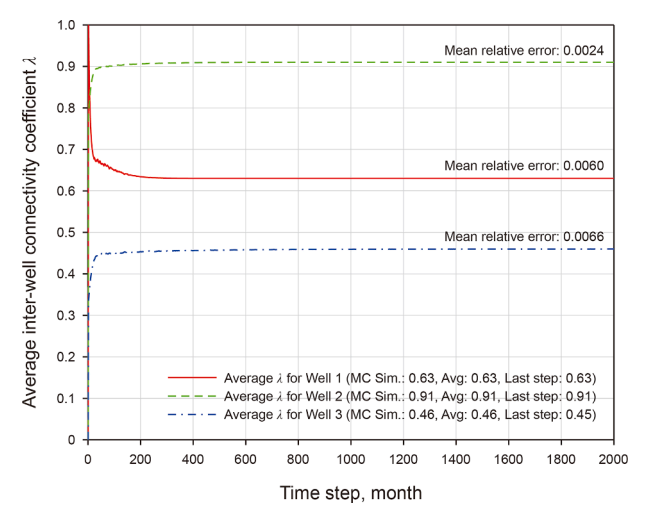
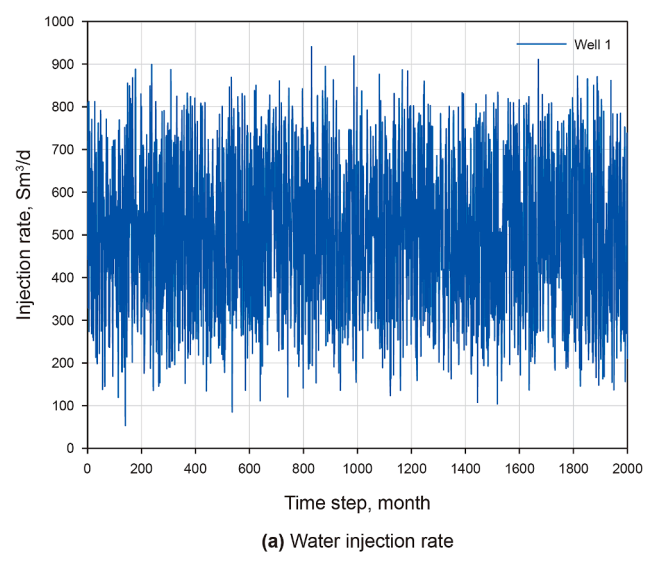


Fig. 9. Plot of the inter-well connectivity coefficient over time of a three-producer-one-injector well group (MC Sim. represents the value of λ for Monte Carlo simulation, Avg represents the average value of λ for the SV-DC model, Last step represents the value of λ for the last time step of the SV-DC model).

d, but due to the inclusion of noise, values outside of this range appear in the dataset. This noise is introduced to simulate the random fluctuations and uncertainty factors that may be encountered in reservoir development, thus making the simulation results closer to the complexity of the actual situation. These generated injection and production data are then utilized to calculate the inter-well connectivity coefficient (Fig. 9) and the time lag coefficient (Fig. 10) through the SV-DC model.

The preset λ' values in the three-producer-one-injector well group are 0.63, 0.91, and 0.46, which are very close to the average and last-time step values calculated by SV-DC model. Note that the horizontal coordinate of Fig. 9 is the simulation time step, so the more steps simulated, the more accurate the results are, and in this sense, it may be more reliable to use the last time step values to evaluate the model performance than the average values. Furthermore, the relative errors of λ calculated according to Eq. (29)



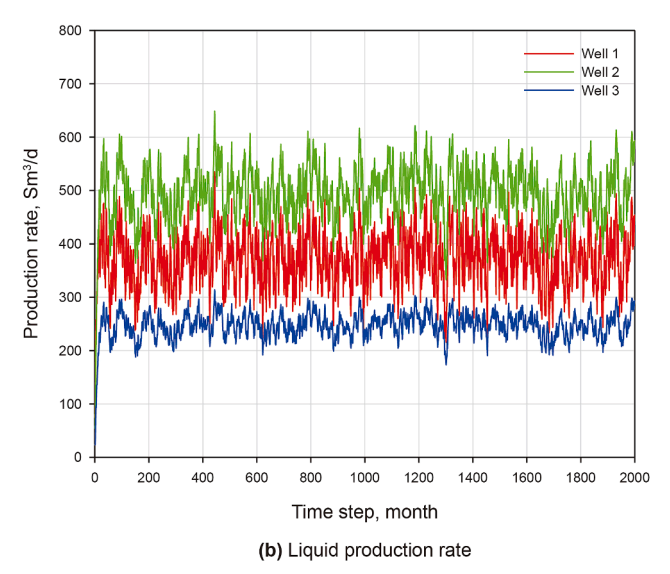


Fig. 8. Water injection rate and liquid production rate from a three-producer-one-injector well group generated by Monte Carlo simulation. The generated data incorporate noise to simulate random fluctuations and uncertainties, reflecting the complexity of actual reservoir conditions.

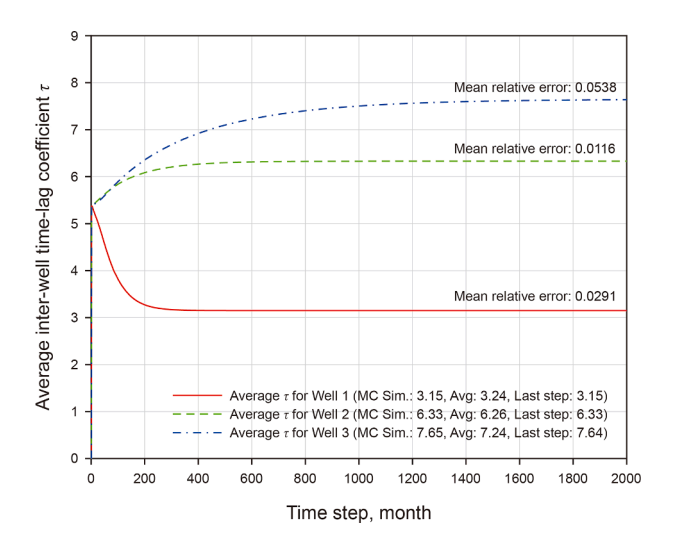


Fig. 10. Plot of the time-lag coefficient over time of a three-producer-one-injector well group in Monte Carlo simulation (MC Sim. represents the value of τ for Monte Carlo simulation, Avg represents the average value of τ for the SV-DC model, Last step represents the value of τ for the last time step of the SV-DC model).

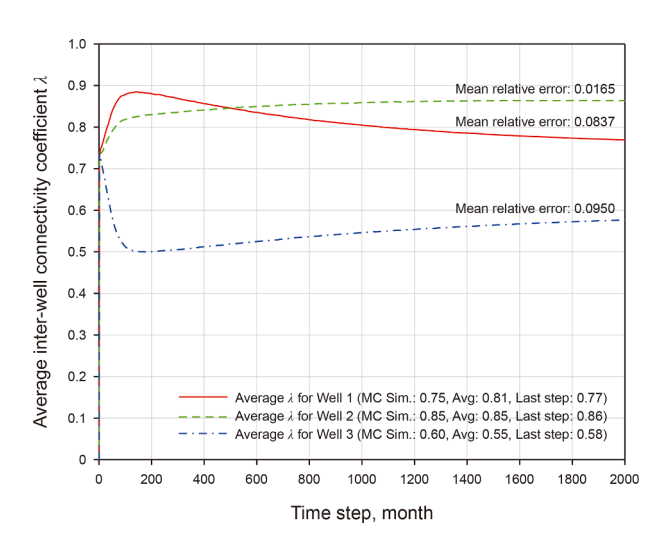


Fig. 11. Plot of the inter-well connectivity over time of a three-injector-one-producer well group in Monte Carlo simulation (MC Sim. represents the value of λ for Monte Carlo simulation, Avg represents the average value of λ for the SV-DC model, Last step represents the value of λ for the last time step of the SV-DC model).

are merely 0.24%, 0.61%, and 0.66%, respectively, which further validates the high robustness of the SV-DC model.

Fig. 10 presents the time-lag coefficient simulation results. The average values using the SV-DC model are 3.24, 6.26, and 7.24, and the values at the last time step are 3.15, 6.33, and 7.65. The relative errors calculated according to Eq. (30) are 5.41%, 1.18%, and 2.97%, respectively.

In summary, for the three-producer-one-injector well group, the relative errors of the inter-well connectivity (0.24%, 0.61%, and 0.66%) and time-lag coefficient (5.41%, 1.18%, and 2.97%) are all within 5.5%. Such a small error range confirms that the SV-DC model possesses high self-consistency and robustness in evaluating the dynamic fluid migration behavior in a multiple well system.

4.2.2. Three injectors and one producer

The same procedures as those used for the three-producer-one-

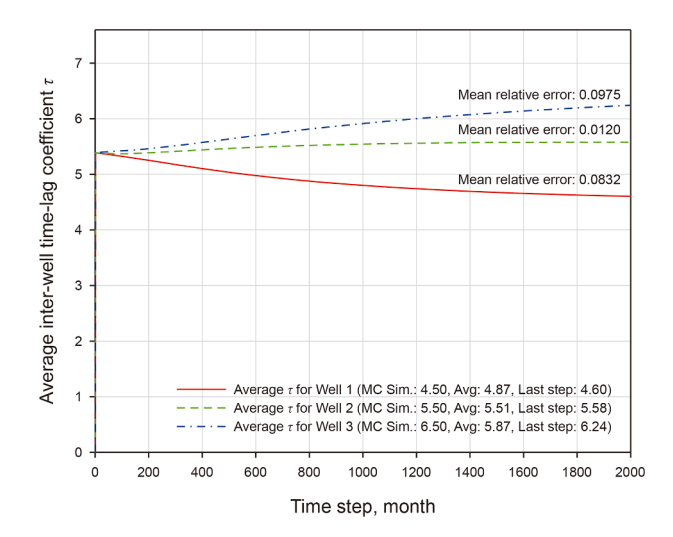


Fig. 12. Plot of the time-lag coefficient over time of a three-injector-one-producer well group in Monte Carlo simulation (MC Sim. represents the value of τ for Monte Carlo simulation, Avg represents the average value of τ for the SV-DC model, Last Step represents the value of τ for the last time step of the SV-DC model).

injector well group were implemented in a three-injector-one-producer well group. First, the Monte Carlo simulation is performed on a three-injector-one-producer well group to generate the injection and production data with noise, and then, calculated by the SV-DC model, the inter-well connectivity coefficient and the time-lag coefficient are obtained in Figs. 11 and 12, respectively.

For the inter-well connectivity coefficients, the preset λ' values in the three-injector-one-producer well group are 0.75, 0.85, 0.60. The relative errors of λ calculated according to Eq. (29) are 1.62%, 8.33%, and 9.46%.

For the time-lag coefficients, the preset τ' values are 4.50, 5.50, and 6.50. The relative errors of τ calculated according to Eq. (30) are 9.74%, 1.20%, and 8.30%. Again, the simulation results indicate a high self-consistency and robustness of the SV-DC model in calculating the inter-well connectivity and time-lag coefficient for a multi-injector-one-producer well group.

It is worth noting that in this study, the "noise" we use primarily consists of randomly generated ideal perturbations aimed at evaluating the adaptability and stability of the model under interfering signals. However, such noise differs from the irregular signals that may occur when the reservoir undergoes drastic changes, and thus the current results do not fully represent the model's performance under more extreme conditions. Nonetheless, by incorporating an EKF into the SV-DC model, we can dynamically calibrate inter-well connectivity parameters at each time step, and the model's robust performance under ideal noise suggests good adaptability to certain levels of fluctuation. In future work, we plan to consider noise types that more closely resemble complex reservoir scenarios-including irregular disturbances arising from significant changes in reservoir behavior—and integrate additional field monitoring data to further assess the model's applicability and reliability.

5. Model field application

To verify the accuracy and reliability of the SV-DC model, comprehensive production data collected from an oilfield being produced in Qinhuangdao was used. Qinhuangdao Oilfield 32-6, located in Bohai Bay, is a large, thick oil field with complex fluvial features, whose main reservoirs are the lower part of the Neoproterozoic Minghuazhen Formation and the upper part of the

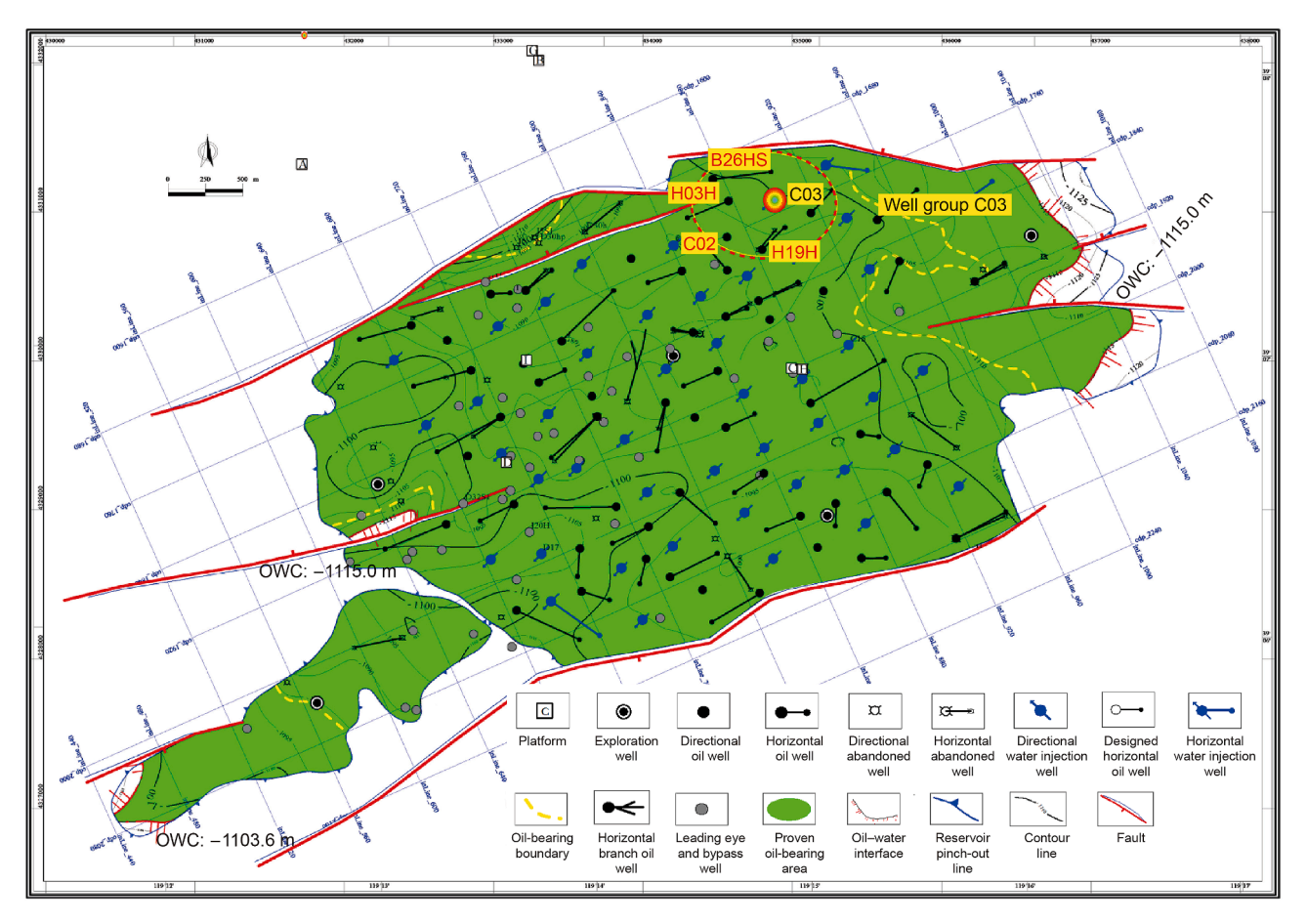


Fig. 13. Schematic diagram of key well groups in the Nml3 sand body in the south zone of Oilfield 32-6.

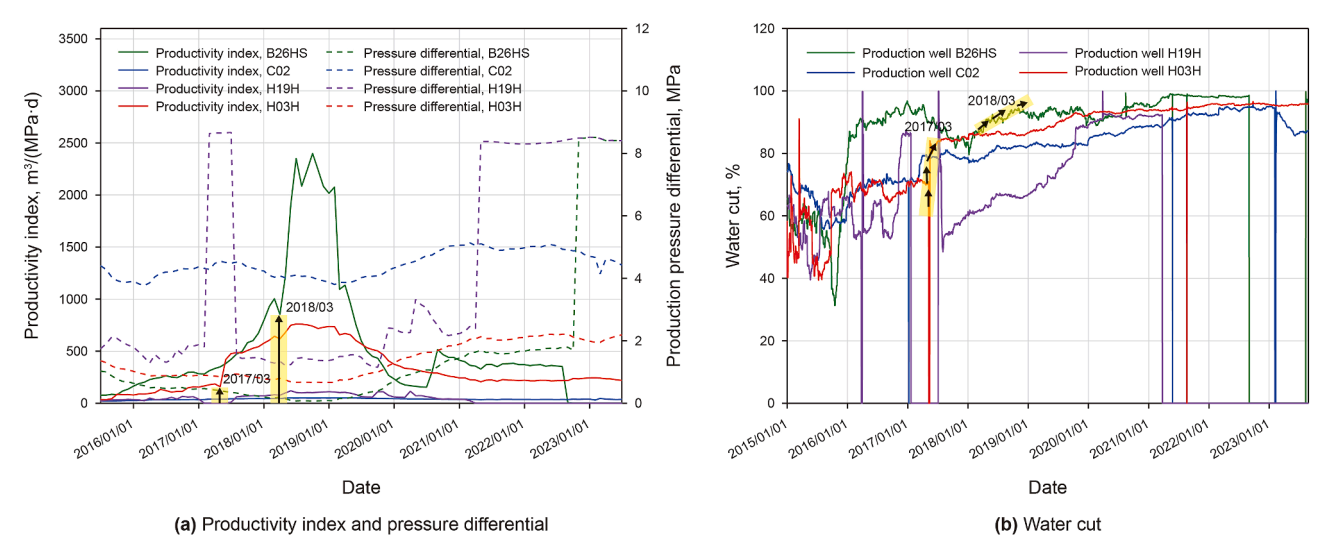


Fig. 14. Development curves of key parameters in Well Group C03.

Guantao Formation. The oilfield is characterized by high porosity (32% on average) and high permeability (2–8474 mD) as well as medium to high crude oil viscosity (22–260 mPa·s).

5.1. Field monitoring for Well Group CO3

Being water flooded for more than 6 decades, the Qinhuangdao

Oilfield is now developing in the extra-high water cut period (> 98%), and the ineffective water circulation (IWC) worsens year by year. Due to the heterogeneity and gravity effect, high permeability channels always exist in the thick reservoir, greatly affecting water flooding efficiency. As shown in Fig. 13, Well Group CO3 of Qinhuangdao Oilfield 32-6 is taken as the case to explore the development of IWC by analyzing the key development

parameters such as the productivity index and water cut. Well Group C03 consists of four production wells (B26HS, C02, H19H, and H03H) and one central injection well (C03). IWCs in oil fields refer to pathways in which the injected water circulates inefficiently or invalidly, especially at stages with ultra-high water cuts. These channels inhibit oil and gas recovery and lead to resource wastage (Han, 2018). Tracer test results, such as tracer arrival time, tracer concentration, and equivalent permeability, are also available and can be used to assess the degree of inter-well connectivity. Finally, based on the λ and τ calculated by the SV-DC model, the dynamic connectivity volume can be estimated, thus identifying IWCs in the Well Group C03.

5.1.1. Productivity index, water cut and pressure differential

In Fig. 14, the production pressure differential is depicted as the difference between the reservoir pressure and the bottomhole flowing pressure. The productivity index refers to the well's ability to produce fluids under a certain pressure differential, measured in cubic meters per day. Water cut of a well refers to the mass or volume of water in the liquid produced from a production well. It is generally accepted that increases in productivity index and water cut in production wells are indicative of water breakthrough, and there is an urgent need for profile control and water plugging (Yang et al., 2021).

Fig. 14 shows the productivity index and water cut of four wells in Well Group C03, among which the rise in productivity index is particularly pronounced in Well H03H and Well B26HS. Between 2017/03 and 2018/03, the productivity indexes of Well H03H and Well B26HS increased dramatically, as marked by the yellow arrows, while the pressure differential did not change much, so the most likely factor is the formation of dominant water breakthrough pathways that show clear signs of ineffective circulation channels.

Correspondingly, the sudden increase in water cut in Well H03H and Well B26HS at the same time points (Fig. 14(b)) further validates the development of IWCs. Therefore, through the dynamic development characteristics of Well Group C03, it can be inferred that Well H03H may develop the IWC in 2017/03, and Well B26HS may develop an IWC in 2018/03.

5.1.2. Tracer test characterization of Well Group C03

Tracer test information for the four selected production wells has been recorded continuously in the field and is summarized in Table 4. The related information includes the tracer arrival time, tracer lasting time, tracer concentration, and reservoir equivalent permeability.

For Well H03H, the tracer arrived on 2019/08/19 and lasted 32 d, with a tracer concentration of 1.05 mg/L. The tracer arrival time of Well H03H is the earliest, which is most likely due to its highest equivalent permeability (14,620 mD), reflecting the well's superior connectivity. A higher permeability typically allows for faster fluid movement, leading to quicker tracer arrival. The relatively higher permeability value indicates the well's capacity to allow fluid to flow more easily, enhancing its connectivity within the reservoir. Overall, the connectivity of Well H03H is the best, followed by Well B26HS and Well C02, and H19H has the poorest connectivity,

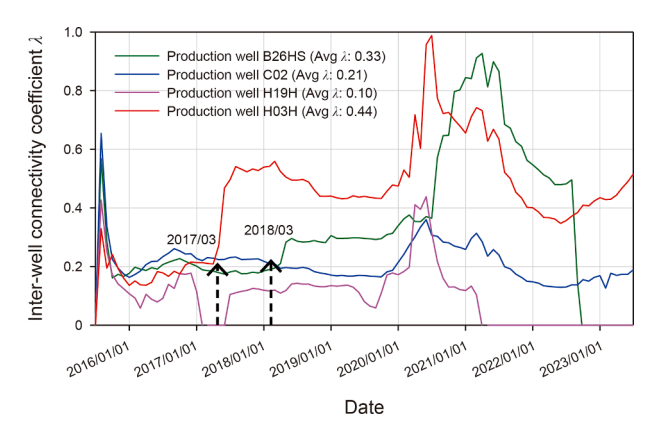


Fig. 15. Inter-well connectivity of Well Group C03 predicted by the SV-DC model. The model predicted inter-well connectivity order, consistent with tracer arrival time results.

which aligns with its lowest permeability (5010 mD). The low permeability of Well H19H likely contributes to the delayed arrival time of the tracer (2019/09/03), as lower permeability zones impede fluid flow, delaying tracer movement through the reservoir.

Well B26HS and Well C02 show intermediate connectivity, supported by their moderate permeabilities (8156 and 7542 mD, respectively) and slightly delayed tracer arrival times (2019/08/24 and 2019/08/25). The moderate permeability values suggest that these wells are in areas where fluid flow is neither too fast nor too slow, thus resulting in a balance between connectivity and tracer arrival time.

The consistent correlation between permeability values and tracer dynamics (arrival time, concentration, and duration) further validates the overall connectivity hierarchy: Well H03H > Well B26HS > Well C02 > Well H19H.

5.2. Model-predicted inter-well connectivity

In Section 5.1, productivity index, water cut, and tracer test information identifying potential IWCs, including the associated well pairs and their development times, are tentatively deduced. To explore the effect of the SV-DC model field application, interwell connectivity is calculated by the SV-DC model and compared with the field information. This task aims to validate the prediction accuracy of the proposed model.

As shown in Fig. 15, the model predicted inter-well connectivity follows the order: $\lambda_{avg(H03H)} > \lambda_{avg(B62HS)} > \lambda_{avg(C02)} > \lambda_{avg(H19H)}$. This pattern is consistent with the tracer test results of tracer arrival time.

Furthermore, the inter-well connectivity increased rapidly for Well H03H in 2017/03 and for Well B62HS in 2018/03, suggesting that IWCs may have formed at those times and that the timing of the development of two IWCs agrees very well with the variation rules of liquid production index, water cut, and tracer test results discussed above.

Table 4Field monitored tracer information for the four selected wells in Well Group C03.

Well group	Well	Tracer arrival time	Tracer lasting time, d	Tracer concentration, mg/L	Equivalent permeability, mD
C03	H03H	2019/08/19	32	1.05	14620
	C02	2019/08/25	38	0.87	7542
	H19H	2019/09/03	47	0.79	5010
	B26HS	2019/08/24	37	1.03	8156

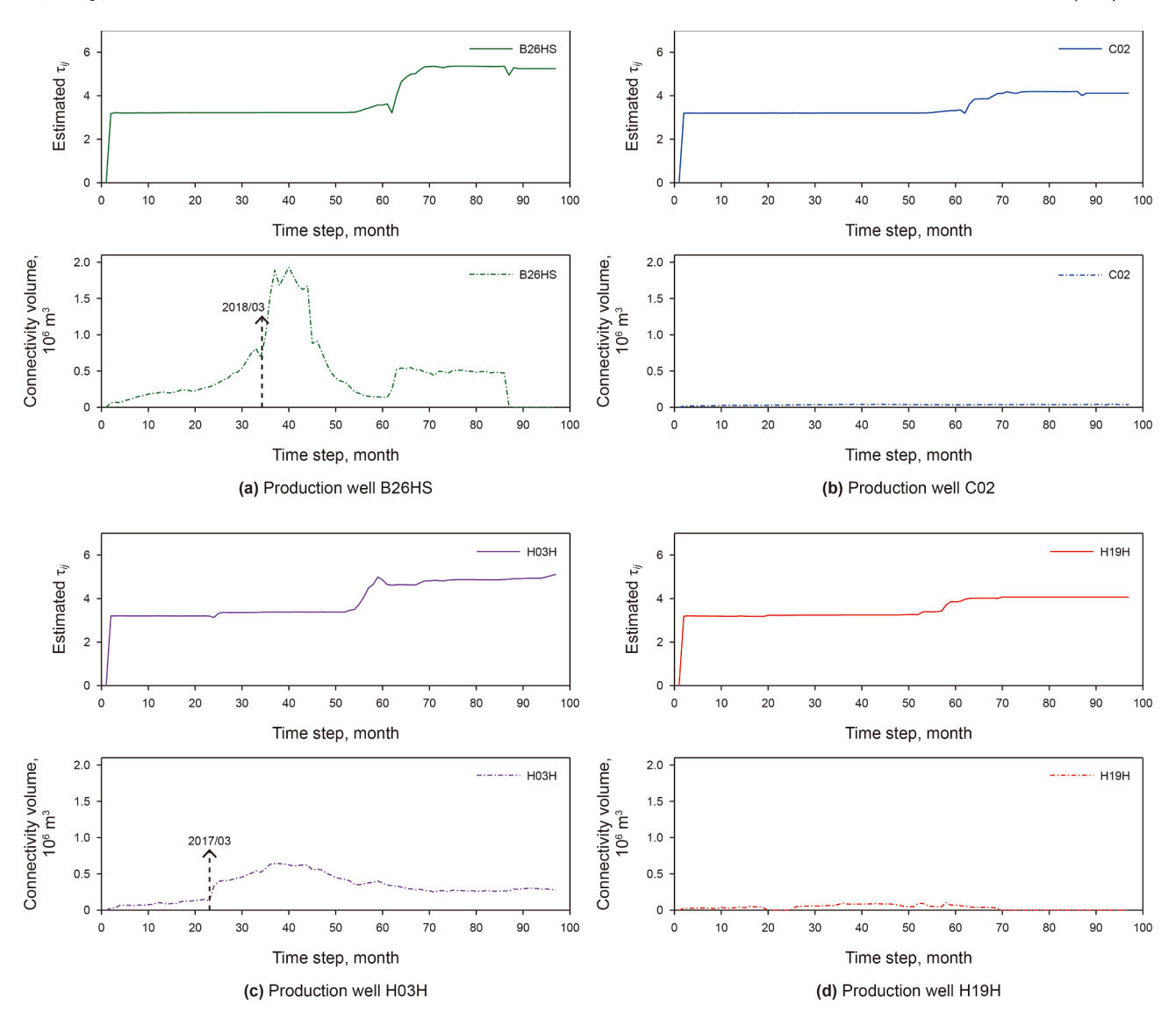


Fig. 16. Plots of time-lag coefficients and connectivity volumes for Well Group CO3.

5.3. Analysis of dynamic connectivity volume

With the time-lag coefficient τ_{ij} directly calculated by the SV-DC model, the dynamic connectivity volume V_{ij} can be obtained by Eq. (6). Connectivity volume is defined as the effective volume between different wells interacting through the reservoir (Vrolijk et al., 2005).

The concept of dynamic connectivity volume introduces a temporal dimension that allows us to track and predict changes in the fluids over time. This dynamic perspective enables an indepth understanding of the reservoir's dynamic behavior and provides a more accurate basis for adjusting the production strategy. The calculation results of the dynamic connectivity volume of Well Group CO3 are shown in Fig. 16.

- (1) Well B26HS shows a peak in connectivity volume in 2018/ 03, suggesting the formation of IWCs, which could point to the opening of dominant water flushing pathways, revealing a key transition in fluid dynamics.
- (2) For Well CO2, the connectivity volume is maintained low, indicating low fluid mobility. The connectivity volume is

- a key metric to quantify the efficiency of fluid mobility, when the connectivity volume is maintained in the range of 0–0.1, it generally reflects limited fluid dynamic connectivity between wells, suggesting that the efficiency of fluid migration from one injector to surrounding producers or neighboring injectors is significantly inhibited. This may be attributed to geologic features of lower permeability or physical isolation or reservoir isolation caused by geologic structural factors such as discontinuous formations or faults.
- (3) The connectivity volume of Well H03H increases dramatically in 2017/03, and this apparent change may reflect fracture initiation or water flushing channel expansion. Such significant dynamic events are critical for reservoir management, indicating potential enhanced reservoir activity or the formation of new fluid flow pathways.
- (4) Well H19H is also in the lower range of connectivity volume, showing a stable and balanced connectivity pattern. This suggests that the connectivity between Well H19H and the reservoir, although limited, remains consistent and does not

show signs of fluid dynamic change, which may indicate stability and continuity of production.

To sum up, the magnitude of the connectivity volume calculated by the SV-DC model directly correlates with fluid flow efficiency between wells and the reservoir. A high connectivity volume indicates strong fluid interaction and easy movement of fluids within the reservoir, while a low connectivity volume suggests potential isolation or restricted fluid flow. This finding may be valuable for optimizing production strategies and developing interventions.

Moreover, Fig. 16 reveals that the connectivity volume of Well H03H experiences a significant increase in 2017/03, and the connectivity volume of Well B62HS shows a similar upward trend in 2018/03. This rule is mutually verified by the above results as discussed in Sections 5.1 and 5.2. The SV-DC model shows its potential in applying connectivity volume analysis to identify and time IWCs. By tracking the time-series changes in the connectivity volume, one can gain more insight into the fluid migration patterns within the reservoir.

Although we have validated the adaptability of the SV-DC model in local well groups in this study, we are also exploring its application across the entire well group in the oilfield. The preliminary results show that the model achieves an accuracy rate of 96%. We are currently organizing this research, and detailed results will be provided in a future paper.

6. Conclusions

This study introduces a state variable-based dynamic capacitance (SV-DC) model, which significantly enhances and extends the traditional capacitance model. By integrating the EKF algorithm, the SV-DC model offers greater flexibility in predicting inter-well connectivity and time-lag coefficients. A key strength of the SV-DC model is its robust ability to handle noise, effectively quantifying prediction uncertainty through a defined covariance matrix. The key innovative contributions of this paper are as follows.

- (1) Based on the production data generated by a commercial simulator, the SV-DC model has been proven to be more sensitive to the applied pressure impulses. The inter-well connectivity coefficients predicted by the SV-DC model and the SV model are closely related to the magnitude of the permeability of the preferential channel. As the permeability increases, the inter-well connectivity increases accordingly.
- (2) The newly proposed SV-DC model in this study reveals the dynamic evolution of the time-lag coefficient, which is inversely proportional to the permeability of the preferential channel. This finding is consistent with the observations in the simulated breakthrough time of the water cone.
- (3) The robustness of the SV-DC model is validated using synthetic data generated through Monte Carlo simulations on two commonly used well patterns. The relative errors of the inter-well connectivity and time-lag coefficients are all below 5.5%, demonstrating the high robustness and stability of the SV-DC model in evaluating fluid migration within a well group.
- (4) The SV-DC model is implemented in Well Group C03 in Qinhuangdao Oilfield 32-6 to explore the development of ineffective circulation channels by analyzing the productivity index and water cut. The rises in productivity index and water cut in Wells H03H and B26HS indicate the development time of ineffective circulation channels,

- combined with the tracer test information, once again confirming the accuracy and reliability of the proposed SV-DC model.
- (5) The connectivity volume calculated by the SV-DC model correlates with the well ability to exchange fluids. A high connectivity volume corresponds to strong fluid interaction, while a low connectivity volume may indicate reservoir isolation or fluid flow restriction.

CRediT authorship contribution statement

Li-Wen Guo: Writing – review & editing, Writing – original draft, Visualization, Validation, Methodology, Investigation, Formal analysis, Data curation, Conceptualization. **Shi-Yuan Qu:** Conceptualization, Data curation, Formal analysis. **Yuan-Yuan Lei:** Conceptualization, Data curation, Formal analysis. **Zhi-Hong Kang:** Conceptualization, Data curation, Formal analysis. **Shuo-Liang Wang:** Visualization, Validation, Supervision, Software, Resources, Project administration, Methodology, Investigation, Funding acquisition, Formal analysis, Data curation, Conceptualization.

Declaration of competing interest

The authors declare that they have no known competing financial interests or personal relationships that could have appeared to influence the work reported in this paper.

Acknowledgements

This research was funded by the National Natural Science Foundation of China (Grant No. 52374051) and by the Joint Fund for Enterprise Innovation and Development of NSFC (Grant No. U24B2037).

References

- Akin, S., 2014. Optimization of reinjection allocation in geothermal fields using capacitance-resistance models. In: Thirty-Ninth Workshop on Geothermal Reservoir Engineering. Stanford University. https://pangea.stanford.edu/ERE/pdf/IGAstandard/SGW/2014/Akin.pdf.
- Artun, E., 2017. Characterizing interwell connectivity in waterflooded reservoirs using data-driven and reduced-physics models: a comparative study. Neural Comput. Appl. 28, 1729–1743. https://doi.org/10.1007/s00521-015-2152-0.
- Cheng, H., Vyatkin, V., Osipov, E., Zeng, P., Yu, H., 2020. LSTM based EFAST global sensitivity analysis for interwell connectivity evaluation using injection and production fluctuation data. IEEE Access 8, 67289–67299. https://doi.org/ 10.1109/ACCESS.2020.2985230.
- Cremon, M.A., Christie, M., Gerritsen, M.G., 2018. Monte Carlo simulation for uncertainty quantification in reservoir simulation: a convergence study. In: ECMOR XVI 16th European Conference on the Mathematics of Oil Recovery. https://doi.org/10.3997/2214-4609.201802226.
- Eshraghi, S.E., Rasaei, M.R., Zendehboudi, S., 2016. Optimization of miscible CO₂ EOR and storage using heuristic methods combined with capacitance/resistance and Gentil fractional flow models. J. Nat. Gas Sci. Eng. 32, 304–318. https://doi.org/10.1016/j.jngse.2016.04.012.
- Gong, M., Zhang, J., Yan, Z., Wang, J., 2021. Prediction of interwell connectivity and interference degree between production wells in a tight gas reservoir. J. Pet. Explor. Prod. Technol. 11, 3301–3310. https://doi.org/10.1007/s13202-021-01150-0.
- Guo, L., Kang, Z., Ding, S., Yuan, X., Yang, H., Zhang, M., Wang, S., 2024. A new algorithm model based on extended Kalman filter for predicting inter-well connectivity. Appl. Sci. 14, 9913. https://doi.org/10.3390/app14219913.
- Han, S., 2018. Research on the identification of inefficient and invalid circulation in ultra-high water cut stage. In: AIP Conf. Proc., 1971, 030018. https://doi.org/10. 1063/1.5041137.
- Hani Binti, A.S., Hendraningrat, L., Idris, N.N., Yakup, M.H., Rinadi, M., Sedaralit, M. F., 2020. Waterflood evaluation and optimisation through rapid interwell connectivity modelling in a complex reservoir. In: Offshore Technology Conference Asia. https://doi.org/10.4043/30337-MS.
- Holanda, R.W. de, Gildin, E., Jensen, J.L., Lake, L.W., Kabir, C.S., 2018. A state-of-theart literature review on capacitance resistance models for reservoir

characterization and performance forecasting. Energies 11, 3368. https://doi.org/10.3390/en11123368.

- Huang, S., Jia, A., Zhang, X., Wang, C., Shi, X., Xu, T., 2023. Application of inter-well connectivity analysis with a data-driven method in the SAGD development of heavy oil reservoirs. Energies 16, 3134. https://doi.org/10.3390/en16073134.
- Huang, Z., Wang, Z., Hu, H., Zhang, S., Liang, Y., Guo, Q., Yao, J., 2023. Dynamic interwell connectivity analysis of multi-layer waterflooding reservoirs based on an improved graph neural network. Pet. Sci. 21 (2), 1062–1080. https://doi. org/10.1016/j.petsci.2023.11.008.
- Izgec, O., Kabir, C.S., 2012. Quantifying reservoir connectivity, in-place volumes, and drainage-area pressures during primary depletion. J. Petrol. Sci. Eng. 81, 7–17. https://doi.org/10.1016/j.petrol.2011.12.015.
- Kang, Z.J., Zhao, H., Zhang, H., Zhang, Y., Li, Y., Sun, H.T., 2014. Research on applied mechanics with reservoir interwell dynamic connectivity model and inversion method in case of shut-in wells. Appl. Mech. Mater. 540, 296–301. https://doi. org/10.4028/www.scientific.net/AMM.540.296.
- Laochamroonvorapongse, R., Kabir, C.S., Lake, L.W., 2014. Performance assessment of miscible and immiscible water-alternating gas floods with simple tools. J. Petrol. Sci. Eng. 122, 18–30. https://doi.org/10.1016/j.petrol.2014.08.012.
- Liu, F., Mendel, J.M., 2007. Forecasting injector-producer relationships from production and injection rates using an extended Kalman filter. In: SPE Annual Technical Conference and Exhibition. https://doi.org/10.2118/110520-MS.
 Liu, X., Qu, X., Jiang, M., Huang, J., Chen, C., 2020. A new method to quantify
- Liu, X., Qu, X., Jiang, M., Huang, J., Chen, C., 2020. A new method to quantify interwell connectivity using performance data and intelligence algorithm. In: International Petroleum Technology Conference. https://doi.org/10.2523/IPTC-20174-MS.
- Llanes, J.D., Viñales, A., Juri, J., 2022. Assisted 3D model construction and facies propagation in Golfo San Jorge Basin reservoirs for modelling EOR. In: SPE Improved Oil Recovery Conference. https://doi.org/10.2118/209400-MS.
- Mwakipunda, G.C., Yang, Z., Guo, C., 2023. Infill drilling optimization for enhanced oil recovery by waterflooding: a simulation study. J. Energy Eng. 149, 04022053. https://doi.org/10.1061/(ASCE)EY.1943-7897.0000860.
- Nguyen, A.P., 2012. Capacitance resistance modeling for primary recovery, water-flood and water-CO₂ flood. In: SPE Annual Technical Conference and Exhibition. https://doi.org/10.2118/147344-MS.
- Nguyen, A.P., Kim, J.S., Lake, L.W., Edgar, T.F., Haynes, B., 2011. Integrated capacitance resistive model for reservoir characterization in primary and secondary recovery. In: SPE Annual Technical Conference and Exhibition. https://doi.org/10.2118/147344-MS.
- Nugroho, M.H., Aslam, B.M., Marhaendrajana, T., 2023. Production optimization in peripheral waterflood field using capacitive resistance model (CRM) with clustering approach, Pandhawa field case study. Journal IATMI. https://journal.iatmi.or.id/index.php/ojs/article/view/415.
- Ogbeiwi, P., Aladeitan, Y., Udebhulu, D., 2018. An approach to waterflood optimization: case study of the reservoir X. J. Pet. Explor. Prod. Technol. 8, 271–289. https://doi.org/10.1007/s13202-017-0368-5.
- Parra, J.E., Samaniego-V, F., Lake, L.W., 2023. Application of the producer-based capacitance resistance model to undersaturated oil reservoirs in primary recovery. SPE J. 28, 2256–2273. https://doi.org/10.2118/214678-PA.
- Parra, J.E., Samaniego-V, F., Lake, L.W., 2024. CRM-aquifer-fractional flow model to characterize oil reservoirs with natural water influx. SPE J. 29, 538–553. https://doi.org/10.2118/217973-PA.
- Rini, D., Latuan, Klea, F., Prajanji, I.G.O.S., 2021. Waterflooding management: challenges and solutions during the injection process to obtain effectively and environmentally based oil recovery in oil and gas industry. IOP Conf. Ser. Earth Environ. Sci. 690, 012037. https://doi.org/10.1088/1755-1315/690/1/012037.
- Sayarpour, M., 2008. Development and application of capacitance-resistive models to water/CO₂ floods. In: SPE Annual Technical Conference and Exhibition. https://doi.org/10.13140/RG.2.1.1798.3847.
- Sayarpour, M., Kabir, C.S., Lake, L.W., 2009. Field applications of capacitance-resistance models in waterfloods. SPE Reservoir Eval. Eng. 12, 853–864. https://doi.org/10.2118/114983-PA.
- Sayarpour, M., Zuluaga, E., Kabir, C.S., Lake, L.W., 2007. The use of capacitance-

- resistive models for rapid estimation of waterflood performance and optimization. In: SPE Annual Technical Conference and Exhibition. https://doi.org/10.2118/110081-MS
- Shan, Y., Wu, Y., Qin, M., Liu, D., Yao, B., 2022. Interwell connectivity study. In: Offshore Technology Conference Asia. https://doi.org/10.4043/31624-MS.
- Sheng, S., Duan, Y., Wei, M., Yue, T., Wu, Z., Tan, L., 2021. Analysis of interwell connectivity of tracer monitoring in carbonate fracture-vuggy reservoir: taking T-well group of Tahe Oilfield as an example. Geofluids, e5572902. https://doi.org/10.1155/2021/5572902
- Tao, Q., Bryant, S.L., 2012. Optimal control of injection/extraction wells for the surface dissolution CO₂ storage strategy. In: Carbon Management Technology Conference. https://doi.org/10.7122/151370-MS.
- Tao, Q., Bryant, S.L., 2013. Optimizing CO₂ storage in a deep saline aquifer with the capacitance-resistance model. Energy Proc. 37, 3919–3926. https://doi.org/10.1016/j.egypro.2013.06.290.
- Tao, Q., Bryant, S.L., 2015. Optimizing carbon sequestration with the capacitance/resistance model. SPE J. 20, 1094–1102. https://doi.org/10.2118/174076-PA.
 Tetteh, J.T., Brady, P.V., Barati Ghahfarokhi, R., 2020. Review of low salinity
- Tetteh, J.T., Brady, P.V., Barati Ghahfarokhi, R., 2020. Review of low salinity waterflooding in carbonate rocks: mechanisms, investigation techniques, and future directions. Adv. Colloid Interface Sci. 284, 102253. https://doi.org/ 10.1016/j.cis.2020.102253
- Thiam, M., Nakhaee, A., 2023. Reservoir interwell connectivity estimation from small datasets using a probabilistic data driven approach and uncertainty quantification. Geoenergy Sci. Eng. 230, 212154. https://doi.org/10.1016/j. geogn.2023.212154.
- Vadapalli, U., Srivastava, R.P., Vedanti, N., Dimri, V.P., 2014. Estimation of permeability of a sandstone reservoir by a fractal and Monte Carlo simulation approach: a case study. Nonlinear Process Geophys. 21, 9–18. https://doi.org/10.5194/npg-21-9-2014.
- Vrolijk, P., James, B., Myers, R., Maynard, J., Sumpter, L., Sweet, M., 2005. Reservoir connectivity analysis-defining reservoir connections and plumbing. In: SPE Middle East Oil and Gas Show and Conference. https://doi.org/10.2118/93577-MS
- Wohl, E., Brierley, G., Cadol, D., Coulthard, T.J., Covino, T., Fryirs, K.A., Grant, G., Hilton, R.G., Lane, S.N., Magilligan, F.J., Meitzen, K.M., Passalacqua, P., Poeppl, R. E., Rathburn, S.L., Sklar, L.S., 2019. Connectivity as an emergent property of geomorphic systems. Earth Surf. Process. Landf. 44, 4–26. https://doi.org/ 10.1002/esp.4434.
- Yang, R., Jiang, R., Guo, S., Chen, H., Tang, S., Duan, R., 2021. Analytical study on the critical water cut for water plugging: water cut increasing control and production enhancement. Energy 214, 119012. https://doi.org/10.1016/j. energy.2020.119012.
- Yousef, A.A., Gentil, P., Jensen, J.L., Lake, L.W., 2006. A capacitance model to infer interwell connectivity from production- and injection-rate fluctuations. SPE Reservoir Eval. Eng. 9, 630–646. https://doi.org/10.2118/95322-PA.
- Zhai, D., Mendel, J.M., 2010. An inequality-constrained extended Kalman filter for continual forecasting of interwell connectivities in waterfloods. In: SPE Western Regional Meeting. https://doi.org/10.2118/134006-MS.
- Zhai, D., Mendel, J.M., Liu, F., 2009. A new method for continual forecasting of interwell connectivity in waterfloods using an extended Kalman filter. In: SPE Western Regional Meeting. https://doi.org/10.2118/121393-MS.
- Zhao, H., Kang, Z., Sun, H., Zhang, X., Li, Y., 2016. An interwell connectivity inversion model for waterflooded multilayer reservoirs. Petrol. Explor. Dev. 43, 106–114. https://doi.org/10.1016/S1876-3804(16)30012-X.
- Zivar, D., Ishanov, A., Pourafshary, P., 2022. Insights into wettability alteration during low-salinity water flooding by capacitance-resistance model. Petroleum Research 7, 500–510. https://doi.org/10.1016/j.ptlrs.2022.01.004.
- Zhang, D., Jiang, W., Kang, Z., Hu, A., Wang, R., 2023. Automatic evaluation of an interwell-connected pattern for fractured-vuggy reservoirs based on static and dynamic analysis. Energies 16, 569. https://doi.org/10.3390/en16010569.
- Zhou, R., Zhang, D., Wei, J., 2022. Experimental investigation on remaining oil distribution and recovery performances after different flooding methods. Fuel 322, 124219. https://doi.org/10.1016/j.fuel.2022.124219.